ON THE DYNAMICS OF FINITE-STRAIN RODS UNDERGOING LARGE MOTIONS - THE THREE-DIMENSIONAL CASE

by

J. C. Simo and L. Vu Quoc

Memorandum No. UCB/ERL M86/11

3 February 1986

COVER

ON THE DYNAMICS OF FINITE-STRAIN RODS UNDERGOING LARGE MOTIONS — THE THREE-DIMENSIONAL CASE

by

J. C. Simo and L. Vu-Quoc

Memorandum No. M86/11

3 February 1986

ELECTRONICS RESEARCH LABORATORY

College of Engineering
University of California, Berkeley
94720

ON THE DYNAMICS OF FINITE-STRAIN RODS UNDERGOING LARGE MOTIONS — THE THREE-DIMENSIONAL CASE

by

J. C. Simo and L. Vu-Quoc

Memorandum No. M86/11

3 February 1986

ELECTRONICS RESEARCH LABORATORY

College of Engineering
University of California, Berkeley
94720

On the Dynamics of Finite-Strain Rods Undergoing Large Motions — The Three-Dimensional Case

J.C. SIMO

Applied Mechanics Division,
Stanford University, Stanford, CA 94305.

and

L. VU-QUOC

Structural Engineering and Structural Mechanics Division,
University of California, Berkeley, CA 94720.

Table of Contents

January 13, 1986

On the Dynamics of Finite-Strain Rods Undergoing Large Motions — The Three-Dimensional Case

J.C. SIMO
Applied Mechanics Division,
Stanford University, Stanford, CA 94305.

L. VU-QUOC
Structural Engineering and Structural Mechanics Division,
University of California, Berkeley, CA 94720.

Abstract

The dynamics of a fully nonlinear rod model, capable of undergoing finite bending, shearing and extension, is considered in detail. Unlike traditional nonlinear structural dynamics formulations, due to the effect of finite rotations the deformation map takes values in $\mathbf{R}^3 \times SO(3)$, which is a differentiable manifold and not a linear space. An implicit time-stepping algorithm that furnishes a canonical extension of the classical Newmark algorithm to the rotation group ($SO(3)$) is developed. In addition to second order accuracy, the proposed algorithm reduces exactly to the plane formulation. Moreover, the exact linearization of the algorithm and associated configuration update is obtained in closed form, leading to a configuration dependent non-symmetric tangent inertia matrix. As a result, quadratic rate of convergence is attained in a Newton-Raphson iterative solution strategy. The generality of the proposed formulation is demonstrated through several numerical examples that include finite vibration, centrifugal stiffening of a fast rotating beam, dynamic instability and snap-through, and large overall motions of a free-free flexible beam.

1. Introduction

The numerical treatment of the dynamic response of a three-dimensional finite-strain rod model formulated in stress resultants is considered in detail. The governing set of nonlinear partial differential equations in the form employed here is given in Simo [1985]. The numerical treatment of these equations restricted to the static problem is considered in Simo & Vu-Quoc [1985a]. We note that the structure of the inertia operator associated with the rotation field of this rod model is identical to the one that typically arises in rigid body mechanics. Related finite-strain rod models developed by Reissner [1972-73,1981-82] and Parker [1979] in a classical context, and by Antman [1974-75] in the context of a director type of formulation, have been restricted to the static problem. These formulations generalize the classical Kirchhoff-Love model (Love [1944]) to account for finite extension and shearing in the rod. In addition, the appropriate parametrization of the configuration space, a question fundamental for computational significance, is not addressed in these developments.

From a computational standpoint, the central issue concerns the treatment of the rotation field which in the present formulation has the same physical meaning as in the classical Kirchhoff-Love model, that is, a one parameter family

of *orthogonal transformations* $\mathbf{A}:[0,L] \rightarrow SO(3)$ of the rotation group $SO(3)$. The basic difficulty lies in the nature of $SO(3)$, a non-commutative Lie group and not a linear vector space. This difficulty is by-passed in the numerical treatment of the Kirchhoff-Love model by Nordgren [1974] by restricting the formulation to cross sections with equal principal inertia and ignoring the effects of rotary inertia. The treatment advocated by Argyris and co-workers [1979,1981a-c,1982] relies on an alternative characterization of the rotation field employing the notion of semi-tangential rotations.

The numerical integration of the rotation field proposed in this paper employs an implicit transient algorithm that furnishes the canonical extension of the Newmark formulae, classically stated in $\mathbf{R}^3$, to the rotation group $SO(3)$. In this extension, notions of differential geometry, such as exponential mapping and parallel transport, play a crucial role. The associated configuration update procedure is amenable to a geometric interpretation consistent with that found in the static problem, Simo & Vu-Quoc [1985a]. Proofs of the convergence and second order accuracy of the algorithm are also given. In addition, *exact* linearization of the proposed algorithm and associated configuration update is obtained in closed form, leading to a *configuration dependent* tangent inertia matrix, which is *non-symmetric* in the rotation degrees of freedom. This exact linearization results in *quadratic* rate of asymptotic convergence in Newton's type of solution strategies. Finally, the proposed time-stepping procedure exactly reduces to the classical Newmark algorithm for the plane problem, as illustrated in our first numerical example presented in section **5**.

The spatial version of the proposed rotation update is related to the procedure proposed by Hughes & Winget [1980], subsequently rephrased in Hughes [1984], and employed by a number of authors in different contexts, including the recent comprehensive work of Stanley [1985]. Although this update procedure and the one proposed in this paper are both second order accurate, the update of the rotation field set forth by Hughes & Winget [1980] does not reduce exactly to the plane problem. In addition, the linearization of the latter update procedure is not addressed by these authors. From a computational stand point both approaches involve essentially the same computational effort.

The formulation developed in this paper encompasses a general class of nonlinear structural dynamics problems that include elastic instability and nonconservative loading, such as follower loads of the circulatory type. A fundamental property of the proposed formulation is that the *proper invariance requirements under superposed rigid body motions*, satisfied by the continuum rod model, are preserved exactly by the integration algorithm and configuration update procedure. In fact, the appropriate invariance of the strain measures along with the inherent conservation of global linear and angular momenta of the

formulation are the essential ingredients for the success of the present approach to the dynamics of flexible beams undergoing large overall motions, Simo & Vu-Quoc [1985b]. Flexible robot arms, rotor blades of aircraft propellers, flexible Earth-orbiting satellites are some typical examples of this type of structures. Traditional approaches to this problem (see, e.g., Laskin *et al* [1983] and Kane *et al* [1985]) assume at the outset small deformation, and rely essentially on the use of a floating frame moving with the deformed structure. A complete review of various types of floating frames can be found in Canavin & Likins [1977]. The equations of motion resulting from these approaches are nonlinear and extensively coupled in the inertia terms because of the Coriolis and centrifugal effects as well as inertia effects due to rotation of the floating frame. By contrast, in Simo & Vu-Quoc [1985b], we refer the dynamics of motion of the beam directly to the inertial frame, thus simplifying considerably the inertia operator. The present paper generalizes these results to the fully three-dimensional case. We note that application of the present algorithm is also of interest in bioengineering (e.g., Mital & King [1979]).

2. Weak form of the governing equations

Notation. Following standard usage, we denote by $SO(3)$ the non-commutative Lie group of proper orthogonal transformations, i.,e.,

$$SO(3) := \{ \mathbf{A} : \mathbf{R}^3 \to \mathbf{R}^3 \text{ linear } | \ \mathbf{A}^T \mathbf{A} = \mathbf{1} , \text{ and } \det \mathbf{A} = 1 \} \quad (2.1)$$

Let $so(3) := \{ \boldsymbol{\Theta} : \mathbf{R}^3 \to \mathbf{R}^3 \text{ linear } | \ \boldsymbol{\Theta} + \boldsymbol{\Theta}^T = \mathbf{0} \}$ be the set of all *skew-symmetric* tensors. In coordinates, relative to a basis $\{\mathbf{e}_i\}$ in $\mathbf{R}^3$, we have $\boldsymbol{\Theta} = \Theta_{ij}\, \mathbf{e}_i \otimes \mathbf{e}_j$ and $\boldsymbol{\theta} = \theta_i\, \mathbf{e}_i$. In matrix notation,

$$[\Theta_{ij}] = \begin{bmatrix} 0 & -\theta_3 & \theta_2 \\ \theta_3 & 0 & -\theta_3 \\ -\theta_2 & \theta_1 & 0 \end{bmatrix} , \quad \{\theta_i\} = \begin{Bmatrix} \theta_1 \\ \theta_2 \\ \theta_3 \end{Bmatrix} \quad (2.2)$$

Recall that $so(3)$ is *isomorphic* to $\mathbf{R}^3$ through the relation $\boldsymbol{\Theta}\, \mathbf{h} = \boldsymbol{\theta} \times \mathbf{h}$, for any $\mathbf{h} \in \mathbf{R}^3$. Here, $\boldsymbol{\theta} \in \mathbf{R}^3$ is the axial vector of $\boldsymbol{\Theta} \in so(3)$. We often use the notation $[\boldsymbol{\theta} \times] := \boldsymbol{\Theta}$. Geometrically, $\mathbf{A} \in SO(3)$ represents a finite rotation. Infinitesimal rotations are *linearized* rotations about the identity. Mathematically, one speaks of $so(3)$ as the tangent space of $SO(3)$ at the identity $\mathbf{1} \in SO(3)$, and employs the notation $so(3) = T_{\mathbf{1}} SO(3)$. Given any $\mathbf{A} \in SO(3)$, and any $\boldsymbol{\Theta} \in so(3)$, $[\boldsymbol{\Theta}\, \mathbf{A}]$ represents an infinitesimal rotation superposed onto a finite rotation represented by $\mathbf{A}$. The set of all superposed infinitesimal rotations $T_{\mathbf{A}} SO(3) := \{ \boldsymbol{\Theta}\, \mathbf{A} \ | \ \text{for } \boldsymbol{\Theta} \in so(3) \}$, is referred to as the *tangent space* at $\mathbf{A} \in SO(3)$. Finally, the straight line $\epsilon \to \epsilon\, \boldsymbol{\Theta}\, \mathbf{A} \in T_{\mathbf{A}} SO(3)$, for $\epsilon > 0$ is mapped by the *exponential map* onto the curve $\epsilon \to \exp[\epsilon\, \boldsymbol{\Theta}]\, \mathbf{A}$.

$= [\sum_{k\geq 0} \frac{\epsilon^k}{k!} \Theta^k]\, \mathbf{A} \in SO(3)$. We recall that for the case of $\Theta \in so(3)$, one has the following explicit formula often credited to Rodrigues

$$\exp[\Theta] = \mathbf{1} + \frac{\sin \|\theta\|}{\|\theta\|}\,\Theta + \frac{1}{2}\,\frac{\sin^2(\|\theta\|/2)}{(\|\theta\|/2)^2}\,\Theta^2 \tag{2.3}$$

2.1. Description of the rod. Local equations

The motion of a rod deforming in the ambient space $\mathbf{R}^3$ is defined through time $t \in \mathbf{R}_+$ as follows. First, the current position of line of centroids of the rod is specified through a map $\phi_o(S, t) : [0, L] \times \mathbf{R}_+ \to \mathbf{R}^3$. Second, the *current orientation* of each cross section $\Omega \in \mathbf{R}^2$ at $S \in [0, L]$, is defined by specifying the orientation of a *moving basis* $\{\mathbf{t}_I(S, t)\}_{\{I=1,2,3\}}$, attached to the cross section, relative to its initial position $\{\mathbf{E}_I\}_{\{I=1,2,3\}}$ at $S \in [0, L]$. That is, by an *orthogonal* transformation $\mathbf{A} : [0, L] \times \mathbf{R}_+ \to SO(3)$ such that $\mathbf{t}_I(S, t) = \mathbf{A}(S, t)\,\mathbf{E}_I$.

The spatial coordinate basis is denoted by $\{\mathbf{e}_i\}_{\{i=1,2,3\}}$, and plays the role of an inertially fixed reference basis. The basis vectors are chosen such that $\{\mathbf{t}_I(S,0)\}_{\{I=1,2,3\}} \equiv \{\mathbf{E}_I\}_{\{I=1,2,3\}} \equiv \{\mathbf{e}_i\}_{\{i=1,2,3\}}$, for $S \in [0,L]$. See Figure 2.1. In coordinates we have $\mathbf{A}(S,t) = \Lambda_{iI}(S,t)\,\mathbf{e}_i \otimes \mathbf{E}_I$

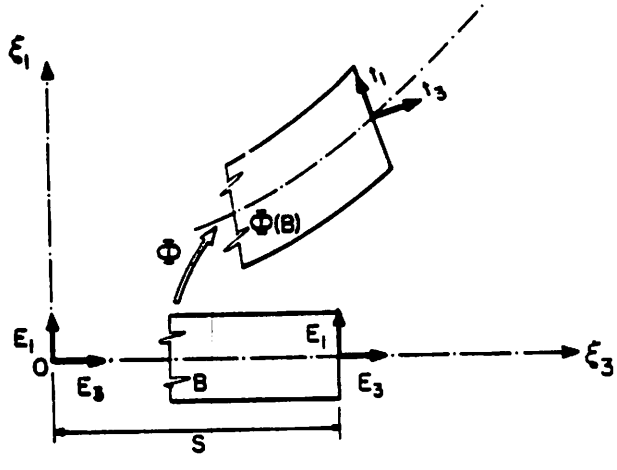

Figure 2.1. *Kinematic description of the rod. Material frame* $\{\mathbf{E}_I\}_{\{I=1,2,3\}}$, *inertial frame* $\{\mathbf{e}_i\}_{i=1,2,3}$, *and cross-section frame* $\{\mathbf{t}_I\}_{\{I=1,2,3\}}$.

The complete system of equations governing the motion of the rod with configuration space defined by (2.3) is summarized in BOX 1 below. Here $C := \{(\phi_o, \mathbf{A}) : [0, L] \to \mathbf{R}^3 \times SO(3)\}$ is the configuration space. $\Omega \equiv -\Omega^T$ defines the spatial curvature of a configuration, i.e., the rate of change of basis $\{\mathbf{t}_I\}$ with respect to the coordinate S, and $\mathbf{W} \equiv -\mathbf{W}^T$ is the spatial spin rate, or

the rate of change of the basis $\{\mathbf{t}_I\}$ with respect to time t. In addition, $\boldsymbol{\omega} \in \mathbf{R}^3$ and $\mathbf{w} \in \mathbf{R}^3$ are *axial vectors* associated with $\boldsymbol{\Omega}$ and $\mathbf{W}$ respectively, that is, $\boldsymbol{\Omega}\,\boldsymbol{\omega} \equiv 0$, and $\mathbf{W}\mathbf{w} \equiv 0$. Finally, $\tilde{\mathbf{n}}$ and $\tilde{\mathbf{m}}$ are the distributed applied force and couple per unit reference length of the rod.

BOX 1. Governing equations for the finite-strain rod. Local form

$$\frac{\partial \mathbf{A}(S,t)}{\partial S} = \boldsymbol{\Omega}(S,t)\,\mathbf{A}(S,t)\,, \qquad \frac{\partial \mathbf{A}(S,t)}{\partial t} = \mathbf{W}(S,t)\,\mathbf{A}(S,t)$$

$$\boldsymbol{\Gamma} = \mathbf{A}^T \frac{\partial \boldsymbol{\phi}_o(S,t)}{\partial S} - \mathbf{E}_3\,, \qquad \boldsymbol{K} = \mathbf{A}^T\,\boldsymbol{\omega}$$

$$\mathbf{n} = \mathbf{A}\,\frac{\partial \psi(S,\boldsymbol{\Gamma},\boldsymbol{K})}{\partial \boldsymbol{\Gamma}}\,, \qquad \mathbf{m} = \mathbf{A}\,\frac{\partial \psi(S,\boldsymbol{\Gamma},\boldsymbol{K})}{\partial \boldsymbol{K}}$$

$$\frac{\partial}{\partial S}\,\mathbf{n} + \tilde{\mathbf{n}} = A_\rho\,\ddot{\boldsymbol{\phi}}_o$$

$$\frac{\partial}{\partial S}\,\mathbf{m} + \frac{\partial \boldsymbol{\phi}_o}{\partial S} \times \mathbf{n} + \tilde{\mathbf{m}} = \mathbf{I}_\rho\,\dot{\mathbf{w}} + \mathbf{w} \times [\mathbf{I}_\rho\,\mathbf{w}]$$

The function $\psi(S, \boldsymbol{\Gamma}, \boldsymbol{K})$ corresponds to the constitutive law relating the strain measures $\boldsymbol{\Gamma}$ and $\boldsymbol{K}$ to the internal forces $\mathbf{n}$ and $\mathbf{m}$. $A_\rho := \int_\Omega \rho_o\, d\Omega$, is the mass per unit length of the beam, where ρ_o is the mass density. If $\overline{\mathbf{I}}_\rho = \overline{\mathrm{J}}_{IJ}\mathbf{E}_I \otimes \mathbf{E}_J$ is the inertia dyadic (constant with respect to time) of the cross section in the reference configuration given by

$$\overline{\mathbf{I}}_\rho := \overline{\mathrm{J}}_{\alpha\beta}\,[\delta_{\alpha\beta}\,\mathbf{1} - \mathbf{E}_\alpha \otimes \mathbf{E}_\beta]\,, \qquad \overline{\mathrm{J}}_{\alpha\beta} := \int_\Omega \rho_o\, X_\alpha\, X_\beta\, d\Omega \tag{2.4}$$

where (X_1, X_2, S) are the coordinates relative to $\{\mathbf{E}_I\}$ of a point in the cross section and $\mathbf{1} := Diag\,[1, 1, 1]$ is the unit tensor, then $\mathbf{I}_\rho$ is the *time dependent* tensor defined as $\mathbf{I}_\rho(S,t) = \mathbf{A}(S,t)\,\overline{\mathbf{I}}_\rho\,\mathbf{A}^T(S,t)$.

2.2. Weak form. Inertia operator

Let $\boldsymbol{\phi} \in C$, denoted by $T_{\boldsymbol{\phi}}C$ be the space of kinematically admissible variations (the tangent space to the configuration space C). Thus, $T_{\boldsymbol{\phi}}C := \{\,\boldsymbol{\eta} \equiv (\boldsymbol{\eta}_0, \boldsymbol{\psi}) : [0, L] \to \mathbf{R}^3 \times \mathbf{R}^3\}$. Multiplying the spatial form of the local balance laws in BOX 1 by an arbitrary *admissible variation* $\boldsymbol{\eta} \in T_{\boldsymbol{\phi}}C$, one obtains

$$G_{dyn}(\boldsymbol{\phi}, \boldsymbol{\eta}) := \int_{[0,L]} \{A_\rho\,\ddot{\boldsymbol{\phi}}_o \cdot \boldsymbol{\eta}_o + [\mathbf{I}_\rho\,\dot{\mathbf{w}} + \mathbf{w} \times (\mathbf{I}_\rho\,\mathbf{w})] \cdot \boldsymbol{\psi}\}\,dS - G(\boldsymbol{\phi}, \boldsymbol{\eta}) \tag{2.5}$$

where $G(\boldsymbol{\phi}, \boldsymbol{\eta})$ is the weak form of the local static equilibrium equations

$$G(\boldsymbol{\phi}, \boldsymbol{\eta}) := \int_{[0,L]} \{ \frac{\partial \psi(S, \boldsymbol{\Gamma}, \boldsymbol{K})}{\partial \boldsymbol{\Gamma}} \bullet \mathbf{A}^T [\frac{\partial \boldsymbol{\eta}_o}{\partial S} - \boldsymbol{\psi} \times \frac{\partial \boldsymbol{\phi}_o}{\partial S}] + \frac{\partial \psi(S, \boldsymbol{\Gamma}, \boldsymbol{K})}{\partial \boldsymbol{K}} \bullet \mathbf{A}^T \frac{\partial \boldsymbol{\psi}}{\partial S} \} dS$$

$$- \int_{[0,L]} (\tilde{\mathbf{n}} \bullet \boldsymbol{\eta}_o + \tilde{\mathbf{m}} \bullet \boldsymbol{\psi}) dS , \qquad (2.6)$$

for arbitrary $\boldsymbol{\eta} \equiv (\boldsymbol{\eta}_o, \boldsymbol{\psi}) \in T_{\boldsymbol{\phi}} C$. For simplicity, we have assumed homogeneous displacement (Dirichlet) boundary conditions.

3. Covariant implicit time-stepping algorithms

In this section we develop an implicit time-stepping algorithm for the time integration of (2.5). The novelty of the proposed approach lies in the treatment of the rotational part which relies crucially on the use of the discrete counterparts of the *exponential map* and *parallel transport* in the orthogonal group $SO(3)$. The algorithm and associated configuration update may be phrased in either a *spatial* or a *material* setting. In the language of rigid body mechanics, the difference amounts to phrasing the formulation in either spatial or body coordinates. The geometric interpretation of the proposed procedure and its implementation are considered in detail.

3.1. Formulation

In line with standard usage, we employ the subscript n to denote the temporal discrete approximate of a time-varying quantity at time t_n; thus for the displacement field $\mathbf{d}_n(S) \cong \boldsymbol{\phi}_o(S,t_n)$, $\mathbf{v}_n(S) \cong \dot{\boldsymbol{\phi}}_0(S,t_n)$, $\mathbf{a}_n(S) \cong \ddot{\boldsymbol{\phi}}_o(S,t_n)$, and for the rotation field $\mathbf{A}_n(S) \cong \mathbf{A}(S,t_n)$, $\mathbf{w}_n(S) \cong \mathbf{w}(S,t_n)$, $\boldsymbol{\alpha}_n(S) \cong \dot{\mathbf{w}}(S,t_n)$. The basic problem concerning the discrete time-stepping update may be formulated as follows. Given a configuration $\boldsymbol{\phi}_n := (\mathbf{d}_n, \mathbf{A}_n) \in C$, its associated linear and angular velocities, $(\mathbf{v}_n, \mathbf{w}_n)$, and linear and angular accelerations $(\mathbf{a}_n, \boldsymbol{\alpha}_n)$, obtain the *updated* configuration $\boldsymbol{\phi}_{n+1} := (\mathbf{d}_{n+1}, \mathbf{A}_{n+1}) \in C$, the associated updated linear and angular velocities $(\mathbf{v}_{n+1}, \mathbf{w}_{n+1})$, and the updated linear and angular acceleration $(\mathbf{a}_{n+1}, \boldsymbol{\alpha}_{n+1})$, in a manner that is (a) *consistent* and (b) *stable* † with (2.5).

To this end, we proposed the algorithm summarized in BOX 2 below. Note that the algorithm for the translational part of the configuration, that is $(S, t) \to \boldsymbol{\phi}_0(S, t) \in \mathbb{R}^3$, is the classical Newmark algorithm of nonlinear

† The notion of stability corresponds essentially to well-posedness of the semi-discrete problem. In the nonlinear case the appropriate concept of stability remains unsettled, and several notions of stability have been proposed (A-stability, spectral stability, stability in the energy sense, stiffly-stable methods, etc...). See, e.g., Hughes [1976], or Belytschko & Hughes [1983].

elastodynamics (see, e.g., Belytschko & Hughes [1983]). The proposed algorithm for the rotational part $(S,\, t) \to \mathbf{A}(S,\, t) \in SO(3)$, in its material version, furnishes the canonical extension of the Newmark formulas to the orthogonal group $SO(3)$.

BOX 2. Covariant implicit time-stepping algorithm

Momentum Balance at t_{n+1}

$$\int_{[0,L]} \{A_\rho\, \mathbf{a}_{n+1} \cdot \boldsymbol{\eta}_o + \mathbf{\Lambda}_{n+1}\, [\overline{\mathbf{I}}_{\rho n+1}\, \overline{\boldsymbol{\alpha}}_{n+1} + \overline{\mathbf{w}}_{n+1} \times (\overline{\mathbf{I}}_{\rho n+1}\, \overline{\mathbf{w}}_{n+1})] \cdot \boldsymbol{\psi}\}\, dS + G(\boldsymbol{\phi}_{n+1},\, \boldsymbol{\eta}) = 0$$

Translation	**Rotation**
$\mathbf{d}_{n+1} = \mathbf{d}_n + \mathbf{u}_n$	$\mathbf{\Lambda}_{n+1} = \mathbf{\Lambda}_n \exp[\,\overline{\boldsymbol{\Theta}}_n]$
$\mathbf{u}_n = h\,\mathbf{v}_n + h^2\,[(\frac{1}{2} - \beta)\,\mathbf{a}_n + \beta\,\mathbf{a}_{n+1}]$	$\overline{\boldsymbol{\Theta}}_n = h\,\overline{\mathbf{W}}_n + h^2\,[(\frac{1}{2} - \beta)\,\overline{\mathbf{A}}_n + \beta\,\overline{\mathbf{A}}_{n+1}]$
$\mathbf{v}_{n+1} = \mathbf{v}_n + h\,[(1 - \gamma)\,\mathbf{a}_n + \gamma\,\mathbf{a}_{n+1}]$	$\overline{\mathbf{W}}_{n+1} = \overline{\mathbf{W}}_n + h\,[(1 - \gamma)\,\overline{\mathbf{A}}_n + \gamma\,\overline{\mathbf{A}}_{n+1}]$

In BOX 2, $\overline{\boldsymbol{\Theta}}$, $\overline{\mathbf{W}}$, $\overline{\mathbf{A}}$ are elements of $so(3)$ (*skew-symmetric* tensors) with components in the basis $\{\mathbf{E}_I\}$. Their axial vectors are denoted respectively by $\overline{\boldsymbol{\theta}}$, $\overline{\mathbf{w}}$, $\overline{\boldsymbol{\alpha}}$, and are elements of $\mathbf{R}^3$. Note that the components of a material object, say $\overline{\boldsymbol{\Theta}}$, in the material basis $\{\mathbf{E}_I\}$ are numerically equal to the components of its spatial counterpart, $\boldsymbol{\Theta} = \mathbf{A}\,\overline{\boldsymbol{\Theta}}\,\mathbf{A}^T$ in the *convected basis* $\{\mathbf{t}_I\}$. The same property holds for the associated axial vectors: $\boldsymbol{\theta} = \mathbf{A}\overline{\boldsymbol{\theta}}$.

Remark 3.1. For the rotation part, since the inertia dyadic has constant components in the material basis $\{\mathbf{E}_I\}$, it is more advantageous to write the time-stepping algorithm for the rotation part in the material setting, as indicated in BOX 2. Note that in the spatial setting, the update of the rotation field is *from the left*, i.e., $\mathbf{A}_{n+1} = \exp[\,\boldsymbol{\Theta}_n]\mathbf{A}_n$. □

Geometric interpretation. Further insight into the nature of the algorithm summarized in BOX 2 is gained by examining its geometric interpretation. For the translational part, the time-stepping procedure is the standard Newmark algorithm and takes place in $\mathbf{R}^3$. Hence, the exponential map reduces to the identity, and the parallel transport is simply a shift of the base point. Pictorially, we have the situation depicted in Figure **3.1(*a*)**.

For the rotation part, the time-stepping procedure takes place in $SO(3)$. A given configuration $\mathbf{A}_n \in SO(3)$ is updated forward in time by exponentiating the incremental rotation $\boldsymbol{\Theta}_n \in so(3)$ to obtain $\mathbf{A}_{n+1} = \exp\,[\boldsymbol{\Theta}_n]\,\mathbf{A}_n$. Since $\overline{\boldsymbol{\Theta}}_n = \mathbf{A}_n^T\,\boldsymbol{\Theta}_n\,\mathbf{A}_n$, it follows from well known properties of the exponential map that $\mathbf{A}_{n+1} = \mathbf{A}_n \exp\,[\overline{\boldsymbol{\Theta}}_n]$, which is the update formula recorded in BOX 2. Such a procedure ensures that $\mathbf{A}_{n+1}$ remains in $SO(3)$ in the natural way by making

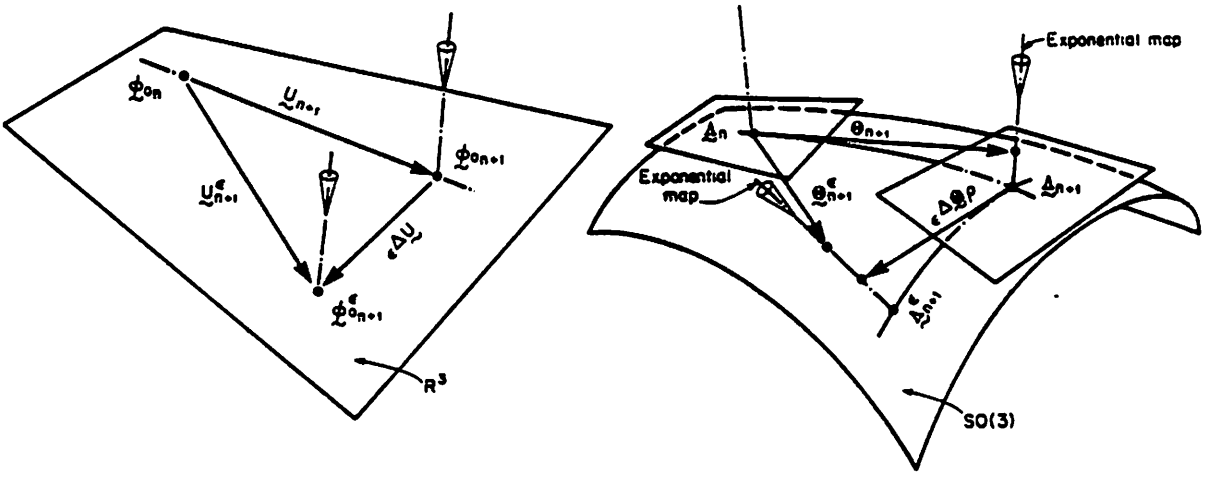

Figure 3.1 *Geometric interpretation of the time-stepping algorithm. (a) Translational part takes place in* $\mathbf{R}^3$. *(b) Rotational part takes place in* $SO(3)$. *Velocity and acceleration update takes place in the same tangent space.*

use of the discrete version of the exponential map. Note that the step forward in time of the angular velocity $\mathbf{W}_n$ and acceleration $\mathbf{A}_n$ is performed with their respective material versions, $\overline{\mathbf{W}}_n$ and $\overline{\mathbf{A}}_n$, in the same tangent space $T_1SO(3)$; the result is then parallel transported to $T_{\mathbf{A}_{n+1}}SO(3)$. The material time-stepping procedure may be thought of as emanating from the following system

$$\dot{\mathbf{A}} = \mathbf{A}\,\overline{\mathbf{W}}\,, \quad \dot{\overline{\mathbf{W}}} = \overline{\mathbf{A}} \tag{3.1}$$

A precise consistency argument is given in Lemma 4.1. □

3.2. Update procedure: Basic setup

The formulae contained in BOX 2 define the velocity $(\mathbf{v}_{n+1}, \mathbf{w}_{n+1})$ and the acceleration $(\mathbf{a}_{n+1}, \boldsymbol{\alpha}_{n+1})$ in terms of the *incremental field* $\Delta\boldsymbol{\phi}_n := (\mathbf{u}_n, \boldsymbol{\theta}_n)$ from the base points $(\mathbf{v}_n, \mathbf{w}_n)$ and $(\mathbf{a}_n, \boldsymbol{\alpha}_n)$. Thus, the weak form of momentum balance at time t_{n+1}, $G_{dyn}(\boldsymbol{\phi}(S, t_{n+1}), \boldsymbol{\eta}(S)) = 0$, depending on velocity and acceleration becomes, by virtue of the time stepping-algorithm, a *nonlinear functional* of the incremental field $\Delta\boldsymbol{\phi}_n$ denoted by $G_{dyn}(\boldsymbol{\phi}_{n+1}, \boldsymbol{\eta})$. The solution of this nonlinear variational equation is accomplished by an iterative scheme of the Newton type, as follows.

Assume that $\boldsymbol{\phi}^{(i)}_{n+1} := (\mathbf{d}^{(i)}_{n+1}, \mathbf{A}^{(i)}_{n+1})$ is known. By solving the linearized weak form about $\boldsymbol{\phi}^{(i)}_{n+1}$, one obtains an *incremental* field $\Delta\boldsymbol{\phi}^{(i)}_{n+1} := (\Delta\boldsymbol{\phi}^{(i)}_{on+1}, \Delta\boldsymbol{\theta}^{(i)}_{n+1})$. The basic setup is: Given $\Delta\boldsymbol{\phi}^{(i)}_{n+1} \in T_{\boldsymbol{\phi}^{(i)}_{n+1}}C$ update $\boldsymbol{\phi}^{(i)}_{n+1} \in C$ to $\boldsymbol{\phi}^{(i+1)}_{n+1} \in C$ in a manner consistent with the time-stepping algorithm in BOX 2. Again the central

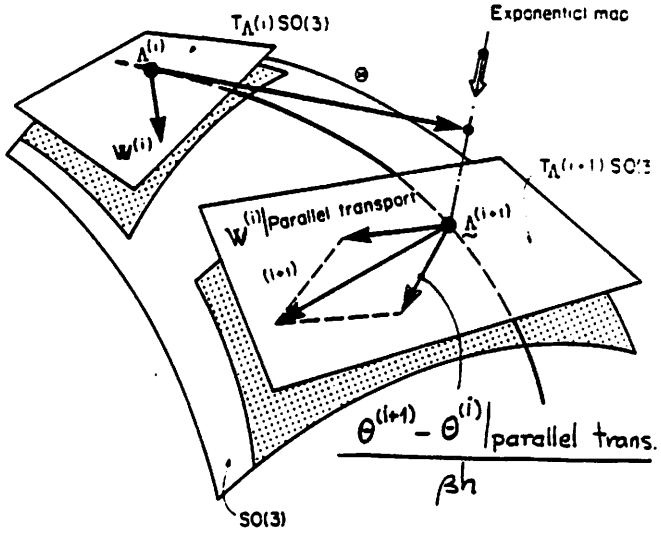

Figure 3.2. *Update procedure for rotational part.*

issue concerns the update of the incremental rotation. First, making use of the exponential, one sets

$$\mathbf{A}_{n+1}^{(i)} = \exp[\boldsymbol{\Theta}_n^{(i)}]\, \mathbf{A}_n\,, \qquad \mathbf{A}_{n+1}^{(i+1)} = \exp[\boldsymbol{\Theta}_n^{(i+1)}]\, \mathbf{A}_n \tag{3.2}$$

Note that (3.2) makes sense since $\boldsymbol{\Theta}_n^{(i)}\, \mathbf{A}_n$ and $\boldsymbol{\Theta}_n^{(i+1)}\, \mathbf{A}_n$ are both in the tangent space $T_{\mathbf{A}_n}SO(3)$. Next, making use of the incremental exponential map we have

$$\mathbf{A}_{n+1}^{(i+1)} = \exp[\Delta\boldsymbol{\Theta}_{n+1}^{(i)}]\, \mathbf{A}_{n+1}^{(i)} \tag{3.3}$$

Again we note that (3.3) makes perfect geometric sense since $\Delta\boldsymbol{\Theta}_{n+1}^{(i)}\mathbf{A}_{n+1}^{(i)}$ is in the tangent space $T_{\mathbf{A}_{n+1}^{(i)}}SO(3)$. Combining (3.2) and (3.3) we obtain the update formulae in BOX 3. A geometric interpretation of the procedure summarized in this box is contained in Figure 3.2.

Remark 3.1. The update procedure in BOX 3 applies for $i \geq 1$. For $i = 0$, the "initial guess" in the Newton process, one sets $\mathbf{d}_{n+1}^{(0)} = \mathbf{d}_n$ and $\mathbf{A}_{n+1}^{(0)} = \mathbf{A}_n$. With this assumption, $(\mathbf{v}_{n+1}^{(0)}, \mathbf{w}_{n+1}^{(0)})$ and $(\mathbf{a}_{n+1}^{(0)}, \boldsymbol{\alpha}_{n+1}^{(0)})$ are then computed by the Newmark formulae given in BOX 2. Alternative starting procedures, such as $(\mathbf{a}_{n+1}^{(0)}, \boldsymbol{\alpha}_{n+1}^{(0)}) = (\mathbf{a}_n, \boldsymbol{\alpha}_n)$, often result in spurious behavior (Taylor [1985]). □

3.3. Exact linearization of the algorithm

We consider the linearization of the temporally discrete weak form $G_{dyn}(\boldsymbol{\phi}_{n+1}, \boldsymbol{\eta})$ about a configuration $\boldsymbol{\phi}_{n+1}^{(i)} = (\mathbf{d}_{n+1}^{(i)}, \mathbf{A}_{n+1}^{(i)}) \in C$ in a manner that is *consistent* with the update procedure summarized in BOX 3. For this purpose, given an incremental field $\Delta\boldsymbol{\phi}_{n+1}^{(i)} = (\Delta\mathbf{u}_{n+1}^{(i)}, \boldsymbol{\theta}_{n+1}^{(i)})$ in the tangent space at $\boldsymbol{\phi}_n^{(i)}$,

BOX 3 Update procedure given $\Delta\boldsymbol{\phi}_{n+1}^{(i)} := (\Delta\mathbf{u}_{n+1}^{(i)}, \Delta\boldsymbol{\theta}_{n+1}^{(i)}) \in T_{\boldsymbol{\phi}_{n+1}^{(i)}} C$

Translation	**Rotation**
$\mathbf{d}_{n+1}^{(i+1)} = \mathbf{d}_{n+1}^{(i)} + \Delta\mathbf{u}_{n+1}^{(i)}$	$\mathbf{\Lambda}_{n+1}^{(i+1)} = \exp\,[\Delta\boldsymbol{\Theta}_{n+1}^{(i)}]\,\mathbf{\Lambda}_{n+1}^{(i)}$
$\mathbf{v}_{n+1}^{(i+1)} = \mathbf{v}_{n+1}^{(i)} + \dfrac{\gamma}{h\beta}\,\Delta\mathbf{u}_{n+1}^{(i)}$	$\exp\,[\boldsymbol{\Theta}_n^{(i+1)}] = \exp\,[\Delta\boldsymbol{\Theta}_{n+1}^{(i)}]\,\exp\,[\boldsymbol{\Theta}_n^{(i)}]$
$\mathbf{a}_{n+1}^{(i+1)} = \mathbf{a}_{n+1}^{(i)} + \dfrac{1}{h^2\beta}\,\Delta\mathbf{u}_{n+1}^{(i)}$	$\overline{\mathbf{w}}_{n+1}^{(i+1)} = \overline{\mathbf{w}}_{n+1}^{(i)} + \dfrac{\gamma}{h\beta}\,[\overline{\boldsymbol{\theta}}_n^{(i+1)} - \overline{\boldsymbol{\theta}}_n^{(i)}]$
	$\overline{\boldsymbol{\alpha}}_{n+1}^{(i+1)} = \overline{\boldsymbol{\alpha}}_{n+1}^{(i)} + \dfrac{1}{h^2\beta}\,[\overline{\boldsymbol{\theta}}_n^{(i+1)} - \overline{\boldsymbol{\theta}}_n^{(i)}]$

we construct a *curve of perturbed configurations* in C, that is, a map $\epsilon \to \boldsymbol{\phi}_{n+1,\epsilon}^{(i)} = (\mathbf{d}_{n+1,\epsilon}^{(i)}, \mathbf{\Lambda}_{n+1,\epsilon}^{(i)}) \in C$, by setting

$$\mathbf{d}_{n+1,\epsilon}^{(i)} := \mathbf{d}_{n+1}^{(i)} + \epsilon\,\Delta\mathbf{u}_{n+1}^{(i)}\,, \qquad \mathbf{\Lambda}_{n+1,\epsilon}^{(i)} := \exp[\,\epsilon\,\Delta\boldsymbol{\Theta}_{n+1}^{(i)}]\,\exp[\boldsymbol{\Theta}_{n+1}^{(i)}]\,\mathbf{\Lambda}_n \tag{3.4}$$

We then define the linearized quantities $(\delta\mathbf{d}_{n+1,\epsilon}^{(i)}, \delta\mathbf{\Lambda}_{n+1,\epsilon}^{(i)})$ at configuration $\boldsymbol{\phi}_{n+1}^{(i)} \in C$, as objects in the tangent space $T_{\boldsymbol{\phi}_{n+1}^{(i)}} C$ given in terms of directional derivative by the expressions

$$\begin{aligned} \delta\mathbf{d}_{n+1}^{(i)} &:= \frac{d}{d\epsilon}\bigg|_{\epsilon=0} \mathbf{d}_{n+1,\epsilon}^{(i)} = \Delta\mathbf{u}_{n+1}^{(i)} \\ \delta\mathbf{\Lambda}_{n+1}^{(i)} &:= \frac{d}{d\epsilon}\bigg|_{\epsilon=0} \mathbf{\Lambda}_{n+1,\epsilon}^{(i)} = \Delta\boldsymbol{\Theta}_{n+1}^{(i)}\,\mathbf{\Lambda}_{n+1}^{(i)} \end{aligned} \tag{3.5}$$

To proceed further with the linearization of the rotation field, we make use of representations for $\mathbf{\Lambda}_{n+1,\epsilon}^{(i)}$ and $\mathbf{\Lambda}_{n+1}^{(i)}$ in terms of exponential maps starting at $\mathbf{\Lambda}_n$. As in (3.2) we have that $\mathbf{\Lambda}_{n+1,\epsilon}^{(i)} = \exp[\boldsymbol{\Theta}_{n,\epsilon}^{(i)}]\,\mathbf{\Lambda}_{n+1}^{(i)}$, where $\boldsymbol{\Theta}_{n,\epsilon}^{(i)}$ and $\boldsymbol{\Theta}_n^{(i)}$ (or more precisely $\boldsymbol{\Theta}_{n,\epsilon}^{(i)}\mathbf{\Lambda}_n$ and $\boldsymbol{\Theta}_n^{(i)}\mathbf{\Lambda}_n$) are in the tangent space $T_{\mathbf{\Lambda}_n} SO(3)$ at $\mathbf{\Lambda}_n$. Note that $\Delta\boldsymbol{\Theta}_{n+1}^{(i)}$ (or more precisely $\Delta\boldsymbol{\Theta}_{n+1}^{(i)}\mathbf{\Lambda}_{n+1}^{(i)}$) belongs to the tangent space $T_{\mathbf{\Lambda}_{n+1}^{(i)}} SO(3)$ at $\mathbf{\Lambda}_{n+1}^{(i)}$. From this representation, along with (3.5) and $(3.2)_1$, we obtain

$$\exp[\,\boldsymbol{\Theta}_{n,\epsilon}^{(i)}] = \exp[\,\epsilon\,\Delta\boldsymbol{\Theta}_{n+1}^{(i)}]\,\exp[\,\boldsymbol{\Theta}_n^{(i)}] \tag{3.6}$$

With this relation in mind, we record below the main result needed in the exact linearization of the weak form in BOX 2. This results is the mathematical statement of the linearization of the *compound rotation* $\boldsymbol{\theta}_{n,\epsilon}^{(i)}$, which is the axial vector of $\boldsymbol{\Theta}_{n,\epsilon}^{(i)}$ in (3.6).

Proposition 3.1. *The linear part of the compound rotation* $\boldsymbol{\theta}_{n,\epsilon}$ *is obtained according to*

$$\delta\boldsymbol{\theta}_n^{(i)} = \left.\frac{d}{d\epsilon}\right|_{\epsilon=0} \boldsymbol{\theta}_{n,\epsilon}^{(i)} = \mathbf{T}(\boldsymbol{\theta}_n^{(i)})\,\Delta\boldsymbol{\theta}_{n+1}^{(i)} \tag{3.7}$$

where $\mathbf{T}$: $T_{\mathbf{A}_{n+1}^{(i)}}SO(3) \to T_{\mathbf{A}_n}SO(3)$ *is a linear map defined by*

$$\mathbf{T}(\boldsymbol{\theta}) := \mathbf{e}\otimes\mathbf{e} + \frac{\|\boldsymbol{\theta}\|/2}{\tan(\|\boldsymbol{\theta}\|/2)}\,[\,\mathbf{1} - \mathbf{e}\otimes\mathbf{e}\,] - \frac{\Theta}{2} \tag{3.8}$$

with $\mathbf{e} := \boldsymbol{\theta}/\|\boldsymbol{\theta}\|$. □

The proof of this proposition is given in appendix I. From (3.7) and the time-stepping algorithm in BOX 3, we obtain the linearization of the angular velocity and acceleration about the configuration $\boldsymbol{\phi}_{n+1}^{(i)}$. The explicit expressions are

$$\delta\overline{\mathbf{w}}_{n+1}^{(i)} = \frac{\gamma}{h\beta}\,\mathbf{A}_n^T\,\mathbf{T}(\boldsymbol{\theta}_n^{(i)})\,\Delta\boldsymbol{\theta}_{n+1}^{(i)}\,, \qquad \delta\overline{\boldsymbol{\alpha}}_{n+1}^{(i)} = \frac{1}{h^2\beta}\,\mathbf{A}_n^T\,\mathbf{T}(\boldsymbol{\theta}_n^{(i)})\,\Delta\boldsymbol{\theta}_{n+1}^{(i)} \tag{3.9}$$

Consider now the linearization of the weak form $G_{dyn}(\boldsymbol{\phi}, \boldsymbol{\eta})$ about the configuration $\boldsymbol{\phi} \equiv \boldsymbol{\phi}_{n+1}^{(i)}$. By definition, we have

$$L[\,G_{dyn}(\boldsymbol{\phi}_{n+1}^{(i)}, \boldsymbol{\eta})\,] = G_{dyn}(\boldsymbol{\phi}_{n+1}^{(i)}, \boldsymbol{\eta}) + \delta G_{dyn}(\boldsymbol{\phi}_{n+1}^{(i)}, \boldsymbol{\eta}) \tag{3.10}$$

where $G_{dyn}(\boldsymbol{\phi}_{n+1}^{(i)}, \boldsymbol{\eta})$ represents the dynamic out-of-balance force, and δG_{dyn} is obtained using the above results of linearization as

$$\begin{aligned}\delta G_{dyn}(\boldsymbol{\phi}_{n+1}^{(i)}, \boldsymbol{\eta}) := {} & \delta G(\boldsymbol{\phi}_{n+1}^{(i)}, \boldsymbol{\eta}) + \frac{1}{h^2\beta}\int_{[0,L]} \boldsymbol{\eta}_o \bullet A_\rho \Delta\mathbf{u}_{n+1}^{(i)}\,dS \\ & + \int_{[0,L]} \boldsymbol{\psi} \bullet \Big[-[\,\mathbf{A}_{n+1}^{(i)}\,\{\,\overline{\mathbf{I}}_\rho\overline{\boldsymbol{\alpha}}_{n+1}^{(i)} + \overline{\mathbf{w}}_{n+1}^{(i)}\times\overline{\mathbf{I}}_\rho\overline{\mathbf{w}}_{n+1}^{(i)}\,\}\times] \\ & + \frac{1}{h^2\beta}\,\mathbf{A}_{n+1}^{(i)}\,\{\,\overline{\mathbf{I}}_\rho - h\gamma\,[\overline{\mathbf{I}}_\rho\overline{\mathbf{w}}_{n+1}^{(i)}\times] + h\gamma\,[\overline{\mathbf{w}}_{n+1}^{(i)}\times]\overline{\mathbf{I}}_\rho\,\}\Big]\,\mathbf{A}_n^T\,\mathbf{T}(\boldsymbol{\theta}_{n+1}^{(i)})\,dS\end{aligned} \tag{3.11}$$

Here, $\delta G(\boldsymbol{\phi}_{n+1}^{(i)}, \boldsymbol{\eta})$ comprises the tangent stiffness operator and, in case of follower load, the tangent load stiffness operator. Detailed expressions for $\delta G(\boldsymbol{\phi}_{n+1}^{(i)}, \boldsymbol{\eta})$ can be found in Simo & Vu-Quoc [1985a]. The tangent inertia matrix, as obtained in (3.11), possesses an unusual characteristic with respect to standard structural dynamics formulations: It is *non-symmetric* and *configuration dependent*. This lack of symmetry concerns only the rotational degrees of freedom and follows from the fact that the deformation map $\boldsymbol{\phi}$ of the configuration space C takes values in the *differentiable manifold* $\mathbf{R}^3\times SO(3)$ rather than in the linear space $\mathbf{R}^3\times\mathbf{R}^3$. The latter typically arises in standard structural dynamics formulations employing infinitesimal rotation field.

4. Spatial discretization: Finite element method

In this section, we shall be concerned with the spatial discretization of the temporally discrete version of the weak form, given in (3.11), employing the finite element method. Section 4.1 focuses on obtaining the tangent inertia matrix, which is a basic feature of the present approach to nonlinear structural dynamics. Detailed expressions for the tangent stiffness matrices are given in Simo & Vu-Quoc [1985a]. In section 4.2, we establish the convergence property of the proposed time-stepping algorithm.

4.1. Tangent inertia matrix

At each configuration $\boldsymbol{\phi}_{n+1}^{(i)} \in C$, we introduce a finite dimensional approximating subspace $V^h \subset T_{\boldsymbol{\phi}_{n+1}^{(i)}} C$ so that the the incremental displacements and rotation field, $\Delta\boldsymbol{\phi}_{n+1}^{(i)}(S) := (\Delta\mathbf{u}_{n+1}^{(i)}, \Delta\boldsymbol{\theta}_{n+1}^{(i)}) \in T_{\boldsymbol{\phi}_{n+1}^{(i)}} C$ are interpolated as

$$\Delta\mathbf{u}_{n+1}^{(i)}(S) \cong \sum_{I=1}^{N} N_I(S)\, \Delta\mathbf{u}_{I,n+1}^{(i)}, \qquad \Delta\boldsymbol{\theta}_{n+1}^{(i)}(S) \cong \sum_{I=1}^{N} N_I(S) \Delta\boldsymbol{\theta}_{I,n+1}^{(i)}, \quad (4.1)$$

where $N_I(S)$ denotes the finite element global function corresponding to node I constructed in the standard manner from the element shape function, and $(\Delta\mathbf{u}_{I,n+1}^{(i)}, \Delta\boldsymbol{\theta}_{I,n+1}^{(i)})$ are the values of $(\Delta\mathbf{u}_{n+1}^{(i)}, \Delta\boldsymbol{\theta}_{n+1}^{(i)})$ at node I. In the standard Galerkin finite element method, we let the admissible variation $\boldsymbol{\eta}(S) = (\boldsymbol{\eta}_o(S), \boldsymbol{\psi}(S))$ be approximated in $V^h \subset T_{\boldsymbol{\phi}_{n+1}^{(i)}} C$ in the same manner as in (4.1). Next, we recall that from a known configuration $\boldsymbol{\phi}_n$ at time t_n, a Newton-Raphson iterative scheme is employed to solve for the configuration $\boldsymbol{\phi}_{n+1}$ at time t_{n+1}. At iteration (i), substitution of the above approximations into the linearized weak form about the configuration $\boldsymbol{\phi}_{n+1}^{(i)}$ yields the following spatially discrete version of the linearized weak form (3.10)

$$L[G_{dyn}(\boldsymbol{\phi}_{n+1}^{(i)}, \boldsymbol{\eta})] \cong \sum_{I=1}^{N} \boldsymbol{\eta}_I \cdot \left\{ \mathbf{P}_I(\boldsymbol{\phi}_{n+1}^{(i)}) + \sum_{J=1}^{N} \mathbf{K}_{IJ}(\mathbf{A}_n, \boldsymbol{\phi}_{n+1}^{(i)})\, \Delta\boldsymbol{\phi}_{J,n+1}^{(i)} \right\} = 0 \quad (4.2a)$$

for any $\boldsymbol{\eta}_I$, where

$$\mathbf{K}_{IJ}(\mathbf{A}_n, \boldsymbol{\phi}_{n+1}^{(i)}) := \mathbf{M}_{IJ}(\mathbf{A}_n, \mathbf{A}_{n+1}^{(i)}) + \mathbf{S}_{IJ}(\boldsymbol{\phi}_{n+1}^{(i)}) + \mathbf{G}_{IJ}(\boldsymbol{\phi}_{n+1}^{(i)}) + \mathbf{L}_{IJ}(\mathbf{A}_{n+1}^{(i)}) \quad (4.2b)$$

In (4.2a), $\mathbf{P}_I(\boldsymbol{\phi}_{n+1}^{(i)})$ represents the residual or out-of-balance force at iteration (i) of the Newton-Raphson scheme. The discrete dynamic tangent operator $\mathbf{K}_{IJ}(\mathbf{A}_n, \boldsymbol{\phi}_{n+1}^{(i)})$ coupling node I and node J is the sum of (i) the tangent inertia matrix $\mathbf{M}_{IJ}(\mathbf{A}_n, \mathbf{A}_{n+1}^{(i)})$, (ii) the tangent material stiffness $\mathbf{S}_{IJ}(\boldsymbol{\phi}_{n+1}^{(i)})$, (iii) the tangent geometric stiffness $\mathbf{G}_{IJ}(\boldsymbol{\phi}_{n+1}^{(i)})$, and (iv) the tangent load stiffness due to follower load $\mathbf{L}_{IJ}(\mathbf{A}_{n+1}^{(i)})$. The incremental displacement and rotation at node J is denoted by $\Delta\boldsymbol{\phi}_{J,n+1}^{(i)} := (\Delta\mathbf{u}_{J,n+1}^{(i)}, \Delta\boldsymbol{\theta}_{J,n+1}^{(i)})$.

From the expression for $\delta G_{dyn}(\boldsymbol{\phi}^{(i)}_{n+1}, \boldsymbol{\eta})$ in (3.11), it follows that the tangent inertia operator takes the form

$$\mathbf{M}_{IJ}(\mathbf{A}_n, \mathbf{A}^{(i)}_{n+1}) = \begin{bmatrix} \mathbf{m}^{(1,1)}_{IJ} & \mathbf{O} \\ \mathbf{O} & \mathbf{m}^{(2,2)}_{IJ}(\mathbf{A}_n, \mathbf{A}^{(i)}_{n+1}) \end{bmatrix} \in \mathbf{R}^{6\times 6} \qquad (4.3a)$$

with

$$\mathbf{m}^{(1,1)}_{IJ} := \frac{1}{h^2\beta} \{ \int_{[0,L]} A_\rho \, N_I(S) \, N_J(S) \, dS \} \, Diag[1, 1, 1] \qquad (4.3b)$$

$$\mathbf{m}^{(2,2)}_{IJ}(\mathbf{A}_n, \mathbf{A}^{(i)}_{n+1}) := \int_{[0,L]} \Big[-[\, \mathbf{A}^{(i)}_{n+1} \{ \overline{\mathbf{I}}_\rho \overline{\boldsymbol{\alpha}}^{(i)}_{n+1} + \overline{\mathbf{w}}^{(i)}_{n+1} \times \overline{\mathbf{I}}_\rho \overline{\mathbf{w}}^{(i)}_{n+1} \} \times] \qquad (4.3c)$$

$$+ \frac{1}{h^2\beta} \mathbf{A}^{(i)}_{n+1} \{ \overline{\mathbf{I}}_\rho - h\gamma [\overline{\mathbf{I}}_\rho \overline{\mathbf{w}}^{(i)}_{n+1} \times] + h\gamma [\overline{\mathbf{w}}^{(i)}_{n+1} \times] \overline{\mathbf{I}}_\rho \} \Big] \mathbf{A}^T_n \, \mathbf{T}(\boldsymbol{\theta}^{(i)}_{n+1}) \, N_I(S) \, N_J(S) \, dS$$

Both $\mathbf{m}^{(1,1)}_{IJ}$ and $\mathbf{m}^{(2,2)}_{IJ}$ are elements of $\mathbf{R}^{3\times 3}$. As noted in section **3**, the tangent inertia matrix is *non-symmetric* and *configuration dependent.* This property concerns only the rotational degrees of freedom as is manifest from the expression for $\mathbf{m}^{(2,2)}_{IJ}(\mathbf{A}_n, \mathbf{A}^{(i)}_{n+1})$. The submatrix $\mathbf{m}^{(1,1)}_{IJ}$ corresponds to the translational degrees of freedom and is constant, as usually found in the expression for the consistent mass matrix when the deformation map takes values in a linear space. We recall that identical property, i.e., the localized character of this non-symmetry, was found as well in the tangent geometric stiffness $\mathbf{G}_{IJ}$ (Simo & Vu-Quoc [1985a]).

4.2. Convergence and accuracy of time-stepping algorithm

The proposed time-stepping algorithm summarized in BOX 2 is proved to be convergent with second order accuracy when $\beta = \frac{1}{4}$ and $\gamma = \frac{1}{2}$. In the case where the deformation map takes values in a linear space, these values of β and γ correspond to the trapezoidal rule with established convergence property (Hughes [1976]).

Lemma 4.1. *Assuming that* $\overline{\mathbf{W}}(t)$ *is twice continuously differentiable, then the algorithm in BOX* **2** *is locally at most third order accurate regardless of the values taken by* β, *i.e.,*

$$\mathbf{A}(t+h) = \mathbf{A}(t) \exp[\, h\overline{\mathbf{W}}(t) + h^2 \{ (\tfrac{1}{2} - \beta)\overline{\mathbf{A}}(t) + \beta\overline{\mathbf{A}}(t+h) \} \,] + \mathbf{O}(h^3) \,, \qquad (4.4)$$

where $\overline{\mathbf{A}}(t) := \dot{\overline{\mathbf{W}}}(t)$. □

The proof of this lemma is given in appendix **I**. With the above result, the convergence property of the algorithm with $\beta = \frac{1}{4}$ and $\gamma = \frac{1}{2}$ is established by

Proposition 4.1. *Consider the system of differential equations* $\dot{\mathbf{A}} = \mathbf{A}\,\overline{\mathbf{W}}$, $\dot{\overline{\mathbf{w}}} = \mathbf{f}(\overline{\mathbf{W}}, \mathbf{A})$ *with* $\mathbf{A} \in SO(3)$ *and* $\overline{\mathbf{w}} \in \mathbf{R}^3$. *Assume that* $\mathbf{f}(\overline{\mathbf{W}}, \mathbf{A})$ *satisfies the Lipschitz condition in* $\overline{\mathbf{W}} \in so(3)$ *and* $\mathbf{A} \in SO(3)$. *The algorithm*

$$\begin{aligned} \mathbf{A}_{n+1} &= \mathbf{A}_n \exp[\, \frac{h}{2}\, \{\overline{\mathbf{W}}_{n+1} + \overline{\mathbf{W}}_n\}\,] \\ \overline{\mathbf{W}}_{n+1} &= \overline{\mathbf{W}}_n + \frac{h}{2}\, \{\overline{\mathbf{A}}_{n+1} + \overline{\mathbf{A}}_n\} \end{aligned} \tag{4.5}$$

is convergent, i.e., $\mathbf{w}_n \to \mathbf{w}(t_n)$ *and* $\mathbf{A}_n \to \mathbf{A}(t_n)$ *as* $h \to 0$, *and second order accurate, provided both* $\overline{\mathbf{w}}(t_n)$ *and* $\overline{\mathbf{w}}_n$ *are bounded.* □

Note that this algorithm is a generalization of the trapezoidal rule to treat the rotation field as expressed in (4.5). The proof of this proposition, given in appendix **I**, is readily extended to the time-stepping algorithm for the dynamics of the three-dimensional rod with $\beta = \frac{1}{4}$ and $\gamma = \frac{1}{2}$. Let $\mathbf{d}^+$ denote the global vector that contains all the nodal displacement degrees of freedom, and similarly for $\mathbf{v}^+$, $\overline{\mathbf{w}}^+$ concerning the linear and angular velocities. On the other hand, $\mathbf{A}^+$ denotes the block diagonal matrix constituted from the $\mathbf{A}$'s at the nodal points.

Proposition 4.2. *Consider the discrete nonlinear structural dynamics problem recast as follows*

$$\begin{aligned} \frac{d}{dt} \begin{Bmatrix} \mathbf{d}^+ \\ \mathbf{v}^+ \\ \overline{\mathbf{w}}^+ \end{Bmatrix} &= \begin{Bmatrix} \mathbf{v}^+ \\ \mathbf{f}_1(\mathbf{d}^+, \mathbf{A}^+) \\ \mathbf{f}_2(\overline{\mathbf{w}}^+, \mathbf{d}^+, \mathbf{A}^+) \end{Bmatrix} \\ \dot{\mathbf{A}}^+ &= (\mathbf{A}\,\overline{\mathbf{W}})^+ \end{aligned} \tag{4.6}$$

Assume that $\mathbf{f}_1$ *and* $\mathbf{f}_2$ *satisfy the Lipschitz condition with respect to the arguments, then* $\mathbf{d}_n^+ \to \mathbf{d}^+(t_n)$, $\mathbf{A}_n^+ \to \mathbf{A}^+(t_n)$, $\mathbf{v}_n^+ \to \mathbf{v}^+(t_n)$, $\overline{\mathbf{w}}_n^+ \to \overline{\mathbf{w}}^+(t_n)$ *as* $h \to 0$ *with second order accuracy, where* $\mathbf{d}_n^+$, $\mathbf{A}_n^+$, $\mathbf{v}_n^+$, *and* $\overline{\mathbf{w}}_n^+$ *are obtained from the time-stepping algorithm described in BOX* 2. □

5. Numerical Examples

In this last section, numerical simulations are presented that involve (i) finite vibration, (ii) fluttering (dynamic instability) due to follower loading, (iii) dynamic snap-through, and (iv) large over all motions of flexible beam structures. Owing to a linearization that is completely consistent with the update procedure, as discussed above, all the numerical simulations exhibit a *quadratic* rate of convergence. The geometric and material properties are selected so that finite deformation occurs during the motion. It is emphasized that the deformed shapes in

all figures reported in this paper are given at the same scale as the geometry of the structures, i.e., there is no magnification of the deformation.

Example 5.1. Spin-up maneuver of a flexible beam. The beam shown in Figure 5.1.1 has one end pinned and the other end free. A prescribed rotation $\psi(t)$ about the axis $\mathbf{e}_3$ is applied at the pinned end as follows

$$\psi(t) = \begin{cases} \dfrac{6}{15}\left[\dfrac{t^2}{2} + \left(\dfrac{15}{2\pi}\right)^2 (\cos\dfrac{2\pi t}{15} - 1)\right] \; rad & 0 \le t \le 15 \quad \text{sec} \\ \\ (6t - 45) \; rad & t > 15 \qquad \text{sec} \end{cases} \tag{5.1}$$

The material properties and finite element mesh used in the simulation are given in Figure 5.1.1. As the beam is spined up from a rest position to a constant angular velocity, it initially bends backward during the accelerated phase as a result of inertia effects. Subsequently, when the angular velocity reaches a constant value of 6 *rad/sec*, the centrifugal force tends to straighten the beam; during this steady-state phase, the beam undergoes small vibration about its nominal position. Several deformed configurations of the beam and time histories of the tip displacements relative the rotating frame are given in Figure 5.1.2. An eigenvalue analysis performed at the reference configuration † yields a period of $T_4 = 0.033$ for the 4th bending mode in the plane of motion. For most of the calculation, we use a time step size of $h = 0.005$ which is about $\frac{1}{7}$th of T_4. It should be noted that during the steady-state motion, the effect of *centrifugal stiffening* tends to increase the natural frequencies. Thus the time step size employed would be in fact larger than one-seventh of the period of the 4th bending mode at this stage. This problem was analyzed by Kane *et al* [1985] and by Simo & Vu-Quoc [1985b] to demonstrate the ability of their respective formulations to capture the centrifugal stiffening effect. Our purpose here is to show that the fully three-dimensional formulation developed in this paper reduces *exactly* to the plane case that was explored in our previous work, i.e., convergence rate and numerical results are *identically* the same in the 3-D case as well as in the 2-D case. □

Example 5.2. Right-angle cantilever beam subject to out-of-plane loading. The right-angle cantilever beam with material properties shown in Figure 5.2.1 is subjected to an out-of-plane concentrated load applied at the elbow. The magnitude of this applied load follows the pattern of a hat function, as shown in Figure 5.2.1. The cantilever undergoes finite free vibration with combined bending and torsion after removal of the applied load; the time histories of

† Note that at the reference configuration, the stiffness and mass matrices are symmetric.

out-of-plane displacements of the elbow and of the tip are given in Figure **5.2.2**. We note that the amplitude of vibration is of the same order of magnitude as the length of each leg of the cantilever. Figure **5.2.3** gives the perspective view of a deformed shape. A linear mode shape analysis of the structure about the reference configuration reveals that the second bending mode of the free-end leg appears as the 10th mode of the structure, with period $T_{10} = 1.6$. This period provides a reasonable estimate for the time step size. Throughout the calculation, we employ a time step size of $h = 0.25$, which is about $\frac{1}{6}$th of T_{10}. The results obtained from a discretization of the cantilever using *two* elements with quadratic interpolation are in good agreement with those obtained from using *ten* elements of the same type. □

Example 5.3. Fluttering of a 45-degree bend under follower load. The static response of the 45-degree bend depicted in Figure **5.3.1** under follower loading was analyzed in Simo & Vu-Quoc [1985b]. In this example, we consider the inertia effects on the response of the bend under follower load that ultimately leads to fluttering (dynamic instability). A follower concentrated force of the circulatory type described in (4.10) is applied at the tip of the bend with steady increase in magnitude at the rate of 100 unit of force per unit of time. Throughout the analysis, we use a time step size of $h = 0.1$. Two perspective views of the deformed shapes are given in Figures **5.3.2** and **5.3.3** to help visualize this complex motion. In Figure **5.3.3**, we also give the path of the tip in the static loading for comparison with the response from dynamic loading. The static loading path is obtained by increments of 50 in the magnitude of the follower load up to a magnitude of 3000. Details of the static analysis has been reported in Simo & Vu-Quoc [1985a]. From Figure **5.3.3**, one can see that initially the dynamic response follows closely the static response. The inertia effects become gradually more pronounced, leading to the divergence of the two paths; then subsequently, dynamic instability sets in to cause strong vibrations of the bend with increasing amplitude and velocity. □

Example 5.4. Out-of-plane dynamic snap-through of a right-angle frame. The right-angle frame depicted in Figure **5.4.1** was analyzed statically in Argyris *et al* [1979] and Simo & Vu-Quoc [1985a]. Here we provide an analysis of this frame accounting for the inertia effects. The degree of freedom at the hinged end are translation along the x direction and rotation about the z direction. The apex of the frame is constrained to lie in the y-z plane. Due to the symmetry of the problem, only half of the frame is modeled employing 10 elements with quadratic interpolation for both displacement and rotation fields. The value of Young's modulus is 71240, and the value of Poisson's ratio is 0.31. The magnitude of the applied moment at the hinged end is chosen to have the same value as the time t. As the magnitude of the applied moment increased, a

perturbed concentrated force is applied at the apex of the frame to induce a lateral motion of the apex. When the moment reaches the critical value of about 615, the loading is removed and the frame snaps through dynamically to the other side as shown in Figure 5.4.2. Figure 5.4.3 reports the time history of the lateral displacement of the apex. In a static analysis, due to the presence of limit points, it is essential to employ a judicious combination of arc-length and displacement control methods in the numerical solution. In a dynamic analysis, such special techniques (continuation methods) are avoided since the mass matrix, as opposed to the tangent stiffness matrix, remains positive definite throughout the entire analysis. The slenderness of the cross-section of the frame with ratio $\frac{height}{thickness} = 50$ causes large amount of twist during the motion. To provide an estimate for the time step size, an eigenvalue analysis is performed at the reference configuration. The first two modes that involve torsional deformation of the leg are the 8th mode and the 11th mode of the structure with period $T_8 = 0.07$ and $T_{11} = 0.03$ respectively. Note that since the frame is very flexible in the out-of-plane direction, frequency modes below the eighth mode are out-of-plane bending modes. A time step size of $h = 0.005$ was selected in the numerical simulation of the dynamic snap-through of the frame. □

Example 5.5. Free-free flexible beam undergoing large overall motion. This problem was first analyzed in the plane case in Simo & Vu-Quoc [1985b]. The beam is initially at an inclined position in the plane ($\mathbf{e}_1$,$\mathbf{e}_2$) as depicted in Figure 5.5.1. A spatially fixed force along $\mathbf{e}_1$ is applied at the lower end denoted by the letter A. Simultaneously, we apply a spatially fixed torque with components along $\mathbf{e}_1$ and along $\mathbf{e}_2$ at end A. The time histories of the magnitude of these applied force and torque are given in Figure 5.5.1. The applied force produce the translational motion; the component along $\mathbf{e}_1$ of the applied torque induces the forward tumbling while its component along $\mathbf{e}_2$ causes the out-of-plane motion of the beam. The resulting three-dimensional motion of the beam follows a periodic "kayak-rowing" pattern. Figure 5.5.2 shows the motion of the beam during the early tumbling stage; the entire sequence of motion is depicted in Figure 5.5.3. The traces of end A and end B of the beam are shown in dotted lines. A side view of the motion in the plane ($\mathbf{e}_2$, $\mathbf{e}_3$) is given in Figure 5.5.4, and a perspective view of the entire sequence of motion in Figure 5.5.5. During the loading stage, finite deformation of the beam is clearly discernible from those Figures. An eigenvalue analysis at the reference configuration of the free-free beam yields a period of vibration of 1.06 for the second bending mode (the first two torsional modes appear at lower frequencies). A time step size of $h = 0.1$ is subsequently chosen for the entire analysis. □

6. Concluding Remarks

Within the context of a general nonlinear finite-strain rod model, we have developed an implicit, second order accurate transient algorithm that furnishes a canonical extension of the classical Newmark algorithm to the rotation group $SO(3)$. The exact linearization of the algorithm and associated configuration update has been obtained in closed form, with accuracy and convergence characteristics precisely stated.

We have demonstrated the generality and effectiveness of the present formulation in several numerical examples involving vibration with finite amplitude, dynamic instability due to follower load, dynamic snap-through fo a thin right-angle frame, and free-free flexible beam subject to large overall motions and undergoing infinitesimal or large deformation. The latter example illustrates the applicability of the proposed formulation to the transient analysis of free-free flexible beam structures undergoing large overall motions. Since the dynamics of the motion is referred directly to the inertial frame, this methodology represents a radical departure from the traditional formulations whereby small deformation is assumed at the outset, and use of a floating frame that moves along with the deformed structure is necessary. In the present approach, the dynamic coupling in the inertia terms that appears by the use of floating frame is exactly accounted for, and nonlinear geometric effects leading to instability are automatically included.

We conclude by noting that the ideas developed in this paper carry over essentially unchanged to the transient analysis of fully nonlinear finite-strain plate and shell models, since they share with the rod model discussed in this paper a common characteristic: the deformation map takes values in the differentiable manifold $\mathbf{R}^3 \times SO(3)$.

Acknowledgements. This work was performed under the auspices of the Air Force Office of Scientific Research. L. Vu-Quoc was supported by grant No. AFOSR-83-0361. This support as well as the encouragement provided by Profs. K.S. Pister, E. Polak, and R.L. Taylor are gratefully acknowledged.

References

Antman, S.S., [1972], "The theory of rods," *Handbuch der Physik,* Vol. VIa/2, Springer-Verlag, Berlin.

Antman, S.S., [1974], "Kirchhoff problem for nonlinearly elastic rods," *Quat. J. Appl. Math.* Vol XXXII, No.3, 221-240.

Antman, S.S., and K. B. Jordan [1975], "Qualitative aspects of the spatial deformation of non-linearly elastic rods," *Proc. Royal Society of Edinburg,* **73***A*, 5,

85-105.

Argyris J.H., H. Balmer, J. St. Doltsinis, P.C. Dunne, M. Haase, M. Kleiber, G.A. Malejannakis, J.P. Mlejenek, M. Muller and D.W. Scharpf [1979], "Finite Element Method -The natural approach," *Comp. Meth. Appl. Mech. Engrg.*, **17/18**, 1-106.

Argyris. J.H. and Sp. Symeonides, [1981a], "Nonlinear finite element analysis of elastic systems under nonconservative loading—Natural formulation. Part I. Quasitatic problems," *Comp. Meth. Appl. Mech. Engrg.* **26**, 75-123.

Argyris. J.H. and Sp. Symeonides, [1981b], "A sequel to: Nonlinear finite element analysis of elastic systems under nonconservative loading -Natural formulation. Part I. Quasitatic problems,: *Comp. Meth. Appl. Mech. Engrg.* **26**, 377-383.

Argyris. J.H. and Sp. Symeonides, [1981c], "Nonlinear finite element analysis of elastic systems under nonconservative loading—Natural formulation. Part II. Dynamic problems," *Comp. Meth. Appl. Mech. Engrg.* **28**, 241-258.

Argyris, J.H., [1982], "An excursion into large rotations," *Comp. Meth. Appl. Mech. Engn.*, **32**, pp.85-155.

Belytschko T., and T.J.R. Hughes, [1983], *Computational Methods for Transient Analysis,* Elsevier Science Publishers.

Canavin, J.R. and P.W. Likins [1977], "Floating reference frames for flexible spacecrafts," *J. of Spacecraft,* 14, No. 12, pp. 724-732.

Hughes, T.J.R. [1976], "Stability, convergence and growth and decay of energy of the average acceleration method in nonlinear structural dynamics," *Computers & Structures,* **6**, pp. 313-324.

Hughes T. J. R., and J. Winget [1980], "Finite rotation effects in numerical integration of rate constitutive equations arising in large-deformation analysis," *Int. J. Num. Meth. Engrg.*, 15

Hughes, T.J.R. [1984], "Numerical Implementation of Constitutive Models: Rate-Independent Deviatoric Plasticity," in *Theoretical Foundations for Large Scale Computations of Nonlinear Material Behavior,* S. Nemat-Nasser, R.J. Asaro and G.A. Hegemier Edts. Martinus Nijhoff Publishers, Dordredch.

Kane, T.R., R.R. Ryan, and A.K. Banerjee [1985], "Dynamics of a beam attached to a moving base," *AAS/AIAA Astrodynamics Specialist Conference,* paper AAS 85-390, Vail, Colorado, August 12-15.

Laskin, R.A., P.W. Likins, and R.W. Longman [1983], "Dynamical equations of a free-free beam subject to large overall motions," *The J. of the Astronautical Sciences,* **31**, No. 4, pp. 507-528.

Love, A.E.H., [1944], *The mathematical theory of elasticity,* Dover Publications, New York.

Mital N.K., and A.I. King [1979], "Computation of rigid-body rotation in three-dimensional space from body-fixed linear acceleration measurements," *J. Applied Mechanics,* **46**, pp. 925-930.

Nordgren, R.P. [1974], "On Computation of the Motion of Elastic Rods," *J. of Applied Mechanics,* pp. 777-780.

Parker, D.F. [1979], "The role of Saint Venant's solutions in rods and beam theories," *J. Applied Mechanics,* **46**, 861-866.

Reissner, E., [1972], "On a one-dimensional finite strain beam theory: The Plane Problem," *J. Appl. Math. Phys.* **23**, pp.795-804.

Reissner, E., [1973], "On a one-dimensional large-displacement finite-strain beam theory," *Studies in Applied Mathematics*, **52**, 87-95.

Reissner, E., [1981], "On finite deformations of space-curved beams," *ZAMP*, **32**, 734-744.

Reissner, E., [1982], "Some remarks on the problem of column buckling," *Ingenieur-Archiv,* **52**, pp.115-119, Springer.

Simo, J.C., K.H. Hjelmstad & R.L. Taylor, [1984], "Numerical formulations for the elasto-viscoplastic response of beams accounting for the effect of shear," *Comp. Meth. Appl. Mech. Engn.*, **42**, pp.301-330.

Simo, J.C. [1985], "A finite strain beam formulation. Part I: The three dimensional dynamic problem," *Comp. Meth. Appl. Mech. Engrg.*, **49**, pp. 55-70.

Simo, J.C., and L. Vu-Quoc [1985a], "Three dimensional finite-strain rod model. Part II: Computational aspects," *Comp. Meth. Appl. Mech. Engrg.*, (in press).

Simo, J.C., and L. Vu-Quoc [1985b], *On the Dynamics of Flexible Beams under Large Overall Motions—The Plane Case*, Electronics Research Laboratory Memorandum No. UCB/ERL M85/63, University of California, Berkeley, August. (Submitted for publication).

Stanley, G. [1985], *Continuum Based Shell Elements,* Ph.D dissertation, Applied Mechanics Division, Stanford University.

Taylor, R.L. [1985], Private communication.

Appendix I: Proof of Proposition 3.1

In order to prove proposition 3.1 we need the following preliminary results

Lemma I.1. *The Frechet derivative of* $\mathbf{e} := \boldsymbol{\theta}/\|\boldsymbol{\theta}\|$ *is given by*

$$D\mathbf{e} = \frac{\mathbf{1} - \mathbf{e}\otimes\mathbf{e}}{\|\boldsymbol{\theta}\|} \tag{I.1}$$

Proof: By taking the directional derivative of $\mathbf{e}$ in the direction $\mathbf{h}$, and noting that $D\|\boldsymbol{\theta}\| = \boldsymbol{\theta}/\|\boldsymbol{\theta}\|$, it follows that $\left.\frac{d}{d\epsilon}\right|_{\epsilon=0} \mathbf{e}_\epsilon := \left.\frac{d}{d\epsilon}\right|_{\epsilon=0} \frac{\boldsymbol{\theta}+\epsilon\mathbf{h}}{\|\boldsymbol{\theta}+\epsilon\mathbf{h}\|}$ $= \frac{\mathbf{h} - (\boldsymbol{\theta}\cdot\mathbf{h})\,\boldsymbol{\theta}/\|\boldsymbol{\theta}\|^2}{\|\boldsymbol{\theta}\|}$, for any $\mathbf{h}\in\mathbf{R}^3$; hence the result. □

Next, we need to obtain the derivative of the exponential map $\exp : T_1SO(3) \to SO(3)$.

Lemma I.2. *Consider the curve in* $so(3)$, $\epsilon \in \mathbf{R} \to \boldsymbol{\Theta}_\epsilon \in so(3)$. *If* $\exp : so(3) \to SO(3)$ *is the exponential map, then its derivative is given by*

$$\frac{d}{d\epsilon}\exp[\,\boldsymbol{\Theta}_\epsilon] = \frac{2}{1+\|\widetilde{\boldsymbol{\theta}}_\epsilon\|^2}\,[\widetilde{\boldsymbol{\Theta}}_\epsilon' + \widetilde{\boldsymbol{\Theta}}_\epsilon\widetilde{\boldsymbol{\Theta}}_\epsilon' - \widetilde{\boldsymbol{\Theta}}_\epsilon'\widetilde{\boldsymbol{\Theta}}_\epsilon]\exp[\,\widetilde{\boldsymbol{\Theta}}_\epsilon] \tag{I.2}$$

where

$$\widetilde{\boldsymbol{\Theta}}_\epsilon := \frac{\tan\left(\|\boldsymbol{\theta}_\epsilon\|/2\right)}{\|\boldsymbol{\theta}_\epsilon\|}\,\boldsymbol{\Theta}_\epsilon \tag{I.3}$$

and $\boldsymbol{\theta}_\epsilon \in \mathbf{R}^3$ *is the axial vector of* $\boldsymbol{\Theta}_\epsilon \in so(3)$.

Proof: See Simo & Vu-Quoc [1985a]. □

With these preliminary results at hand, we now proceed to prove the result concerning the linearization of the compound rotation.

Proof of proposition 3.1. To simplify the notation we omit the subindex $n+1$ and the superindex (i) in what follows. The basic relation in BOX **2** then reads

$$\exp[\,\boldsymbol{\Theta}_\epsilon] = \exp[\,\epsilon\,\Delta\boldsymbol{\Theta}]\,\exp\,[\,\boldsymbol{\Theta}]$$

Differentiating this expression with respect to $\epsilon \in \mathbf{R}$ and setting $\epsilon = 0$, making use of Lemma **I.2** and expressing the final result in terms of axial vectors leads to

$$\frac{2}{1+\|\widetilde{\boldsymbol{\theta}}\|^2}\,[\delta\widetilde{\boldsymbol{\theta}} + \widetilde{\boldsymbol{\theta}} \times \delta\widetilde{\boldsymbol{\theta}}] \;=\; \Delta\boldsymbol{\theta}$$

where $\widetilde{\boldsymbol{\theta}}_\epsilon$ is given by (I.3) and we have set $\widetilde{\boldsymbol{\theta}} = \widetilde{\boldsymbol{\theta}}_\epsilon\Big|_{\epsilon=0}$. Expressed in operator notation, the above equation reads

$$\mathbf{Y}^{-1}(\widetilde{\boldsymbol{\Theta}})\,\delta\widetilde{\boldsymbol{\theta}} = \Delta\boldsymbol{\theta}\,, \quad \text{where} \quad \mathbf{Y}^{-1}(\widetilde{\boldsymbol{\Theta}}) := \frac{1}{1+\|\widetilde{\boldsymbol{\theta}}\|}\,[\mathbf{1} + \widetilde{\boldsymbol{\Theta}}] \tag{I.4}$$

Inversion of $\mathbf{Y}^{-1}(\widetilde{\boldsymbol{\Theta}})$ yields

$$\mathbf{Y}(\widetilde{\boldsymbol{\Theta}}) = \tfrac{1}{2}\,[(1+\|\widetilde{\boldsymbol{\theta}}\|^2)\,\mathbf{1} - \widetilde{\boldsymbol{\Theta}} + \widetilde{\boldsymbol{\Theta}}^2] \equiv \tfrac{1}{2}\,[\mathbf{1} - \widetilde{\boldsymbol{\Theta}} + \widetilde{\boldsymbol{\theta}} \otimes \widetilde{\boldsymbol{\theta}}]$$

Equivalently, making use of (I.3) we may rephrase this expression as

$$\mathbf{Y}(\boldsymbol{\Theta}) = \tfrac{1}{2}\,[\mathbf{1} - \frac{\tan\left(\|\boldsymbol{\theta}\|/2\right)}{\|\boldsymbol{\theta}\|}\,\boldsymbol{\Theta} + \frac{\tan\left(\|\boldsymbol{\theta}\|^2\right)}{\|\boldsymbol{\theta}\|^2}\,\boldsymbol{\theta} \otimes \boldsymbol{\theta}] \tag{I.5}$$

In addition, by differentiating the expression $\widetilde{\boldsymbol{\theta}}_\epsilon = \dfrac{\tan\left(\|\boldsymbol{\theta}_\epsilon\|/2\right)}{\|\boldsymbol{\theta}_\epsilon\|}\,\boldsymbol{\theta}_\epsilon$ with respect to ϵ with the aid of Lemma **I.1**, we obtain

$$\delta\boldsymbol{\theta} = \mathbf{Z}(\boldsymbol{\Theta})\,\delta\widetilde{\boldsymbol{\theta}}\,, \tag{I.6}$$

for $\epsilon = 0$, where $\mathbf{Z}(\boldsymbol{\Theta})$ is given by

$$\mathbf{Z}(\boldsymbol{\Theta}) \;=\; \frac{2}{1+\tan^2(\|\boldsymbol{\theta}\|/2)}\,\mathbf{e}\otimes\mathbf{e} + \frac{2\,\|\boldsymbol{\theta}\|}{\tan\left(\|\boldsymbol{\theta}\|/2\right)}\,[\mathbf{1} - \mathbf{e}\otimes\mathbf{e}] \tag{I.7}$$

Thus, from (I.4) and (I.6) it follows that

$$\delta\boldsymbol{\theta} = \mathbf{Z}(\boldsymbol{\Theta})\,\mathbf{Y}(\boldsymbol{\Theta})\,\Delta\boldsymbol{\theta} \equiv \mathbf{T}(\boldsymbol{\Theta})\,\Delta\boldsymbol{\theta}$$

where, from (I.5) and (I.7), $\mathbf{T}(\boldsymbol{\Theta}) \equiv \mathbf{Z}(\boldsymbol{\Theta})\,\mathbf{Y}(\boldsymbol{\Theta})$ is given by

$$\mathbf{T}(\boldsymbol{\theta}) \;=\; \mathbf{e}\otimes\mathbf{e} + \frac{\|\boldsymbol{\theta}\|/2}{\tan(\|\boldsymbol{\theta}\|/2)}\,[\mathbf{1} - \mathbf{e}\otimes\mathbf{e}] - \frac{\boldsymbol{\Theta}}{2} \qquad \square$$

Appendix II: Convergence and accuracy proofs

Proof of Lemma 4.1. Consider the expressions of $\mathbf{A}(t+h)$ given by the Taylor series expansion,

$$\mathbf{A}(t+h) = \sum_{k \geq 0} \frac{h^k}{k!} \frac{d^k}{dt^k} \mathbf{A}(t) , \tag{II.1}$$

and by the proposed time-stepping algorithm

$$\mathbf{A}(t+h) = \widetilde{\mathbf{A}}(h) = \mathbf{A}(t) \exp[\, h\overline{\mathbf{W}}(t) + h^2 \{(\tfrac{1}{2} - \beta)\overline{\mathbf{A}}(t) + \beta\overline{\mathbf{A}}(t+h)\} \,] \tag{II.2}$$

The consistency and local third order accuracy of algorithm (II.2) follow from the identities

$$\frac{d^k}{dh^k} \widetilde{\mathbf{A}}(h)\bigg|_{h=0} \equiv \frac{d^k}{dt^k} \mathbf{A}(t) , \quad \text{for } k=0,1,2. \tag{II.3a}$$

and

$$\frac{d^3}{dh^3} \widetilde{\mathbf{A}}(h)\bigg|_{h=0} \neq \frac{d^3}{dt^3} \mathbf{A}(t) , \tag{II.3b}$$

regardless of the values taken by β. □

Proof of Proposition 4.1. Let the error measures on $\mathbf{A}$ and $\overline{\mathbf{w}}$ be defined as $\xi_n := \mathbf{A}(t_n) - \mathbf{A}_n$, and $\varsigma_n := \overline{\mathbf{W}}(t_n) - \overline{\mathbf{W}}_n$. Also let $\|\overline{\mathbf{W}}\| := \|\overline{\mathbf{w}}\|$. From Lemma 4.1, and the local third order accuracy of the trapezoidal rule in relation with $(4.5)_2$, i.e.,

$$\overline{\mathbf{W}}(t_{n+1}) - \overline{\mathbf{W}}(t_n) = \frac{h}{2} [\, \mathbf{f}(\overline{\mathbf{W}}(t_{n+1}), \mathbf{A}(t_{n+1})) + \mathbf{f}(\overline{\mathbf{W}}(t_n), \mathbf{A}(t_n)) \,] + \mathbf{O}(h^3) \tag{II.4}$$

we obtain the following recurrence relations for ξ_{k+1} and ς_{k+1}

$$\xi_{k+1} = \xi_k + [\, \mathbf{A}(t_k)(\mathbf{R}_k + \tfrac{1}{2}\mathbf{R}_k^2) - \mathbf{A}_k(\mathbf{S}_k + \tfrac{1}{2}\mathbf{S}_k^2) \,] + \mathbf{O}(h^3) \tag{II.5a}$$

$$\varsigma_{k+1} = \varsigma_k + \frac{h}{2} [\, \overline{\mathbf{A}}(t_{k+1}) - \overline{\mathbf{A}}_{k+1} + \overline{\mathbf{A}}(t_k) - \overline{\mathbf{A}}_k \,] + \mathbf{O}(h^3) \tag{II.5b}$$

where we define $\mathbf{R}_k$ and $\mathbf{S}_k$ to be

$$\mathbf{R}_k := \frac{h}{2} \{\, \overline{\mathbf{W}}(t_{k+1}) + \overline{\mathbf{W}}(t_k) \,\} \tag{II.5c}$$

$$\mathbf{S}_k := \frac{h}{2} \{\, \overline{\mathbf{W}}_{k+1} + \overline{\mathbf{W}}_k \,\} \tag{II.5d}$$

Note that in (II.5a), we have expanded the exponential $\exp[\mathbf{R}_k]$ and $\exp[\mathbf{S}_k]$ in series and retained terms up to order h^2; higher order terms of the form $\frac{\mathbf{R}_n^k}{k!}$ with bounded norm are lumped together in $\mathbf{O}(h^3)$. Next, sum up the relations (II.5a) and (II.5b) for $k = 1,\ldots,n$ to obtain

$$\xi_{n+1} = \sum_{i=0}^{n} [\, \mathbf{A}(t_i)(\mathbf{R}_i + \tfrac{1}{2}\mathbf{R}_i^2) - \mathbf{A}_i(\mathbf{S}_i + \tfrac{1}{2}\mathbf{S}_i^2) \,] + \mathbf{O}(h^2) \tag{II.6a}$$

$$\varsigma_{n+1} = \frac{h}{2}(\overline{\mathbf{A}}(t_{n+1}) - \overline{\mathbf{A}}_{n+1}) + h\sum_{i=1}^{n}(\overline{\mathbf{A}}(t_n) - \overline{\mathbf{A}}_n) + \mathbf{O}(h^2) \tag{II.6b}$$

assuming that there is no initial error, i.e., $\boldsymbol{\xi}_0 = \boldsymbol{\varsigma}_0 = 0$. Since $\dot{\overline{\mathbf{A}}} = \mathbf{f}(\overline{\mathbf{W}}, \overline{\mathbf{A}})$ satisfies the Lipschitz condition with respect to its arguments, taking the norm of (II.6a-b), we have

$$\|\boldsymbol{\xi}_{n+1}\| \leq \sum_{i=1}^{n} \|\mathbf{A}(t_i)(\mathbf{R}_i + \tfrac{1}{2}\mathbf{R}_i^2) - \mathbf{A}_i(\mathbf{S}_i + \tfrac{1}{2}\mathbf{S}_i^2)\| + c_1 h^2 \tag{II.7a}$$

$$\|\boldsymbol{\varsigma}_{n+1}\| \leq \frac{hL}{2}(\|\boldsymbol{\varsigma}_{n+1}\| + \|\boldsymbol{\xi}_{n+1}\|) + hL\sum_{i=1}^{n}(\|\boldsymbol{\varsigma}_i\| + \|\boldsymbol{\xi}_i\|) + c_2 h^2 \tag{II.7b}$$

where c_1 and c_2 are constants and L is the Lipschitz constant. Now note that

$$\begin{aligned}\|\mathbf{A}(t_i)\mathbf{R}_i - \mathbf{A}_i\mathbf{S}_i\| &\leq \|\mathbf{A}(t_i)\|\,\|\mathbf{R}_i - \mathbf{S}_i + \mathbf{S}_i - \mathbf{A}^T(t_i)\mathbf{A}_i\mathbf{S}_i\| \\ &\leq \|\mathbf{R}_i - \mathbf{S}_i\| + \|\mathbf{1} - \mathbf{A}^T(t_i)\mathbf{A}_i\|\,\|\mathbf{S}_i\| \\ &\leq \frac{h}{2}(\|\boldsymbol{\varsigma}_{i+1}\| + \|\boldsymbol{\varsigma}_i\|) + hK_1\|\boldsymbol{\xi}_i\| \end{aligned} \tag{II.8a}$$

and similarly

$$\begin{aligned}\|\mathbf{A}(t_i)\mathbf{R}_i^2 - \mathbf{A}_i\mathbf{S}_i^2\| &\leq \|\mathbf{R}_i^2 - \mathbf{S}_i^2\| + \|\mathbf{1} - \mathbf{A}^T(t_i)\mathbf{A}_i\|\,\|\mathbf{S}_i^2\| \\ &\leq \|\mathbf{R}_i^2 - \mathbf{S}_i^2\| + h^2K_2\|\boldsymbol{\xi}_i\| \,. \end{aligned} \tag{II.8b}$$

where K_1, K_2 are constants. Moreover, we have

$$\begin{aligned}\|\mathbf{R}_i^2 - \mathbf{S}_i^2\| &\leq \|\mathbf{R}_i + \mathbf{S}_i\|\,\|\mathbf{R}_i - \mathbf{S}_i\| + \|\mathbf{R}_i\mathbf{S}_i - \mathbf{S}_i\mathbf{R}_i\| \\ &\leq hK_3\|\boldsymbol{\varsigma}_{i+1} + \boldsymbol{\varsigma}_i\| + \|\mathbf{r}_i \times \mathbf{s}_i\| \\ &\leq (hK_3 + \tfrac{1}{2}h^2K_1)\,(\|\boldsymbol{\varsigma}_{i+1}\| + \|\boldsymbol{\varsigma}_i\|) \end{aligned} \tag{II8.c}$$

in which $\mathbf{r}_i$ and $\mathbf{s}_i$ are the axial vectors of $\mathbf{R}_i$ and of $\mathbf{S}_i$ respectively, and K_3 is a constant. In the above inequalities, we have used the assumption that $\|\overline{\mathbf{w}}(t_n)\|$ and $\|\overline{\mathbf{w}}_n\|$ are bounded. There results

$$\|\boldsymbol{\xi}_{n+1}\| + \|\boldsymbol{\varsigma}_{n+1}\| \leq C_1(h)h^2 + C_2(h)\sum_{i=1}^{n}(\|\boldsymbol{\xi}_i\| + \|\boldsymbol{\varsigma}_i\|) \tag{II.9}$$

in which $C_1(h) = (1 + P(h))^{-1}$ is of order 1 when $h \to 0$, and $P(h)$ and $C_2(h)$ are some polynomials of h. From (II.9), it follows that

$$\|\boldsymbol{\xi}_{n+1}\| + \|\boldsymbol{\varsigma}_{n+1}\| \leq h^2 C_1(h)\,\exp[C_2(h)] \tag{II.10}$$

Thus, $\mathbf{A}_n \to \mathbf{A}(t_n)$ and $\overline{\mathbf{w}}_n \to \overline{\mathbf{w}}(t_n)$ as $h \to 0$ and the rate of convergence is of second order. □

Proof of Proposition 4.2. This proof is similar to the above one, and hence will not be reproduced. □

Figure Captions

Figure 2.1. Kinematic description of the rod. Material frame $\{\mathbf{E}_I\}_{\{I=1,2,3\}}$, inertial frame $\{\mathbf{e}_i\}_{i=1,2,3}$, and cross-section frame $\{\mathbf{t}_I\}_{\{I=1,2,3\}}$.

Figure 3.1. Geometric interpretation of the time-stepping algorithm. (a) Translational part takes place in $\mathbf{R}^3$. (b) Rotational part takes place in $SO(3)$. Velocity and acceleration update takes place *in the same tangent space.*

Figure 3.2. Update procedure for rotational part.

Figure 5.1.1. *Spin-up maneuver.* Problem data.

Figure 5.1.2. *Spin-up maneuver.* Several deflected shapes during first revolution. Time histories for displacement components and section rotation relative to the shadow beam. Time step size $h = 0.005$.

Figure 5.2.1 *Right angle cantilever beam* subject to out-of-plane loading. Problem data.

Figure 5.2.2 *Right angle cantilever beam* subject to out-of-plane loading. Time histories of elbow displacements; Line A: 2 elements, line B: 10 elements. Time histories of tip displcement; Line C: 2 elements, line D: 10 quadratic elements.

Figure 5.2.3 *Right angle cantilever beam* subject to out-of-plane loading. Perspective view of deformed shape.

Figure 5.3.1 *Fluttering of a 45-degree bend* under follower load. Problem data.

Figure 5.3.2 *Fluttering of a 45-degree bend* under follower load. Perspective view of deformed shape from viewpoint A.

Figure 5.3.3 *Fluttering of a 45-degree bend* under follower load. Perspective view of deformed shape from viewpoint B.

Figure 5.4.1 *Out-of-plane dynamic snap-through of a right-angle frame.* Problem data.

Figure 5.4.2 *Out-of-plane dynamic snap-through of a right-angle frame.* Time history of lateral apex displacement.

Figure 5.4.3 *Out-of-plane dynamic snap-through of a right-angle frame.* Perspective view of deformed shapes.

Figure 5.5.1 *Free-free flexible beam undergoing large overall motions.* Problem data.

Figure 5.5.2 *Free-free flexible beam undergoing large overall motions.* Early tumbling stage.

Figure 5.5.3 *Free-free flexible beam undergoing large overall motions.* Entire sequence of motion.

Figure 5.5.4 *Free-free flexible beam undergoing large overall motions.* Side view of deformed shapes.

Figure 5.5.5 *Free-free flexible beam undergoing large overall motions.* Perspective view of deformed shapes.

Material Properties

$EA = 2.8 \times 10^7$

$GA_s = 1 \times 10^7$

$EI = 1.4 \times 10^4$

$A\rho = 1.2$

$I\rho = 6 \times 10^{-4}$

F.E. Mesh: 4 quadratic elements

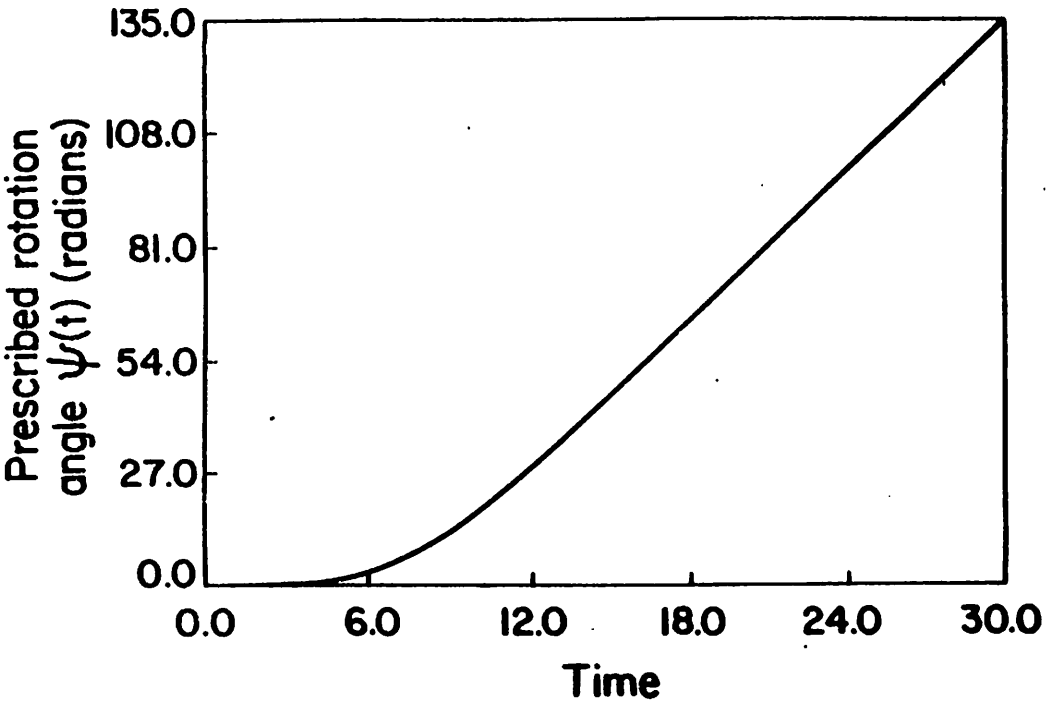

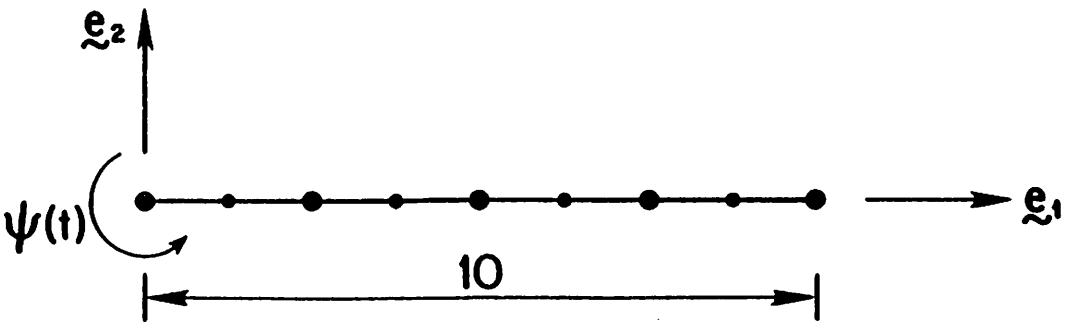

Figure 5.1.1. *Spin-up maneuver.* Problem data.

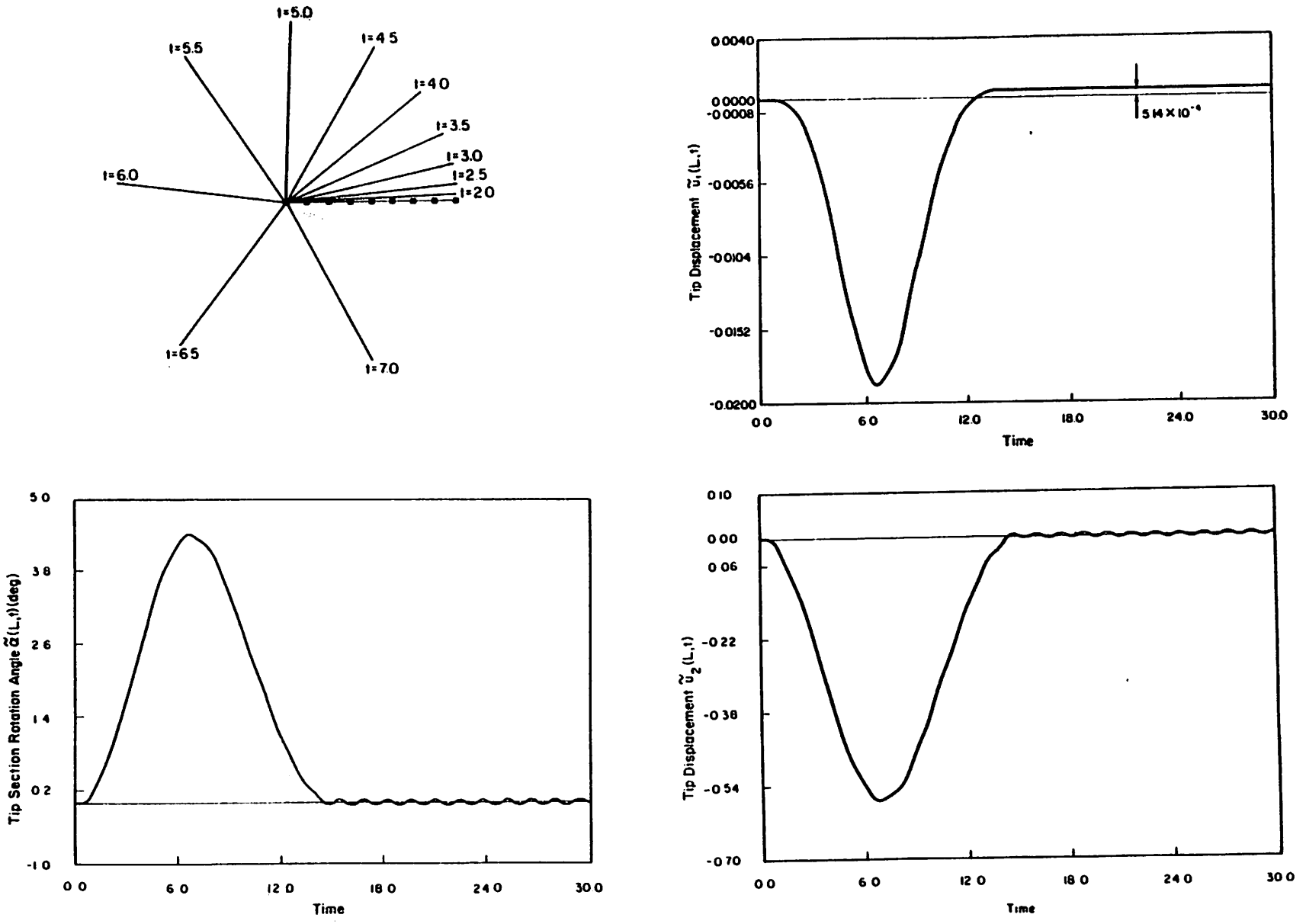

Figure 5.1.2. *Spin-up maneuver.* Several deflected shapes during first revolution. Time histories for displacement components and section rotation relative to the shadow beam. Time step size $h = 0.005$.

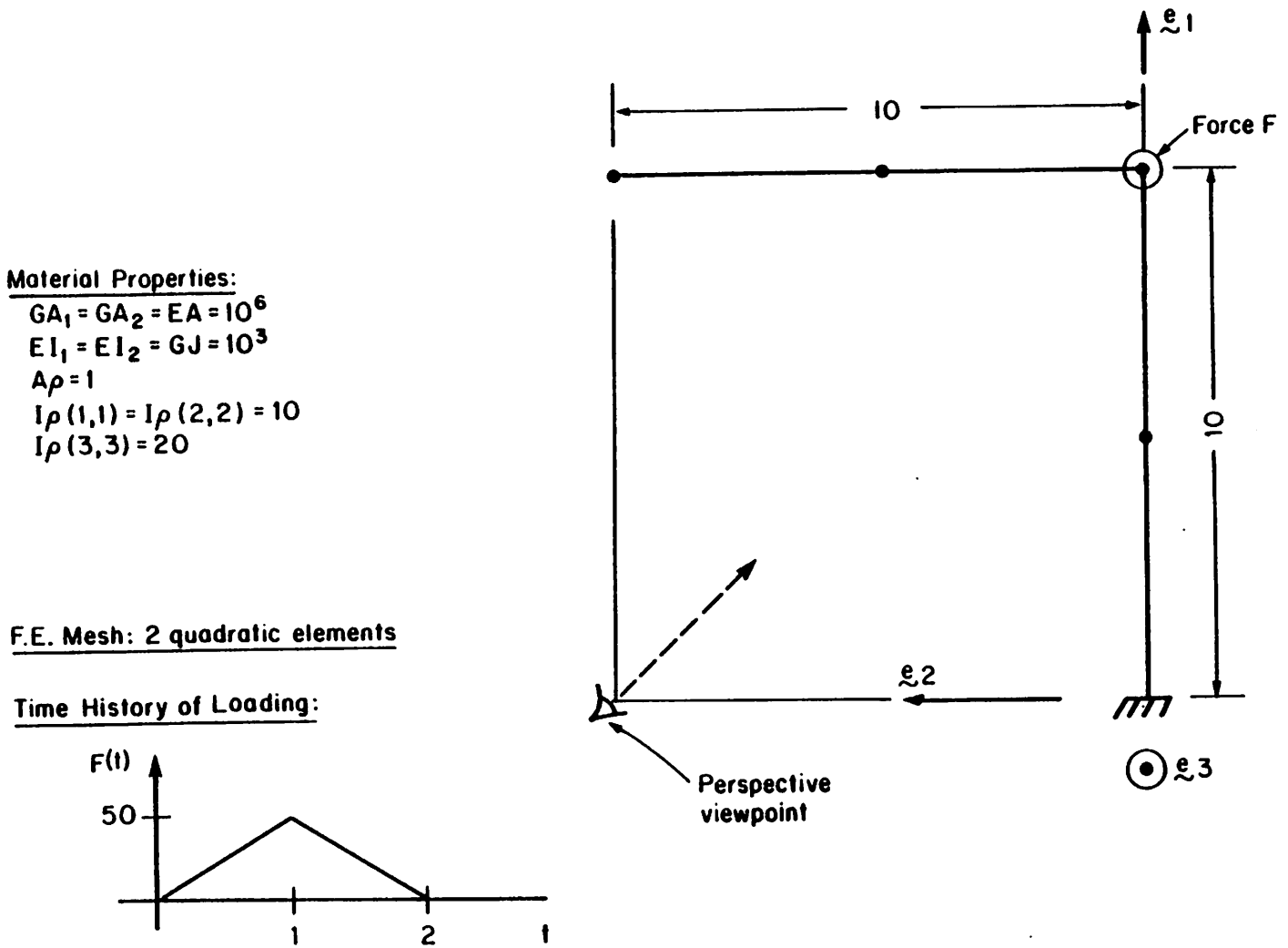

Figure 5.2.1 *Right angle cantilever beam* subject to out-of-plane loading. Problem data.

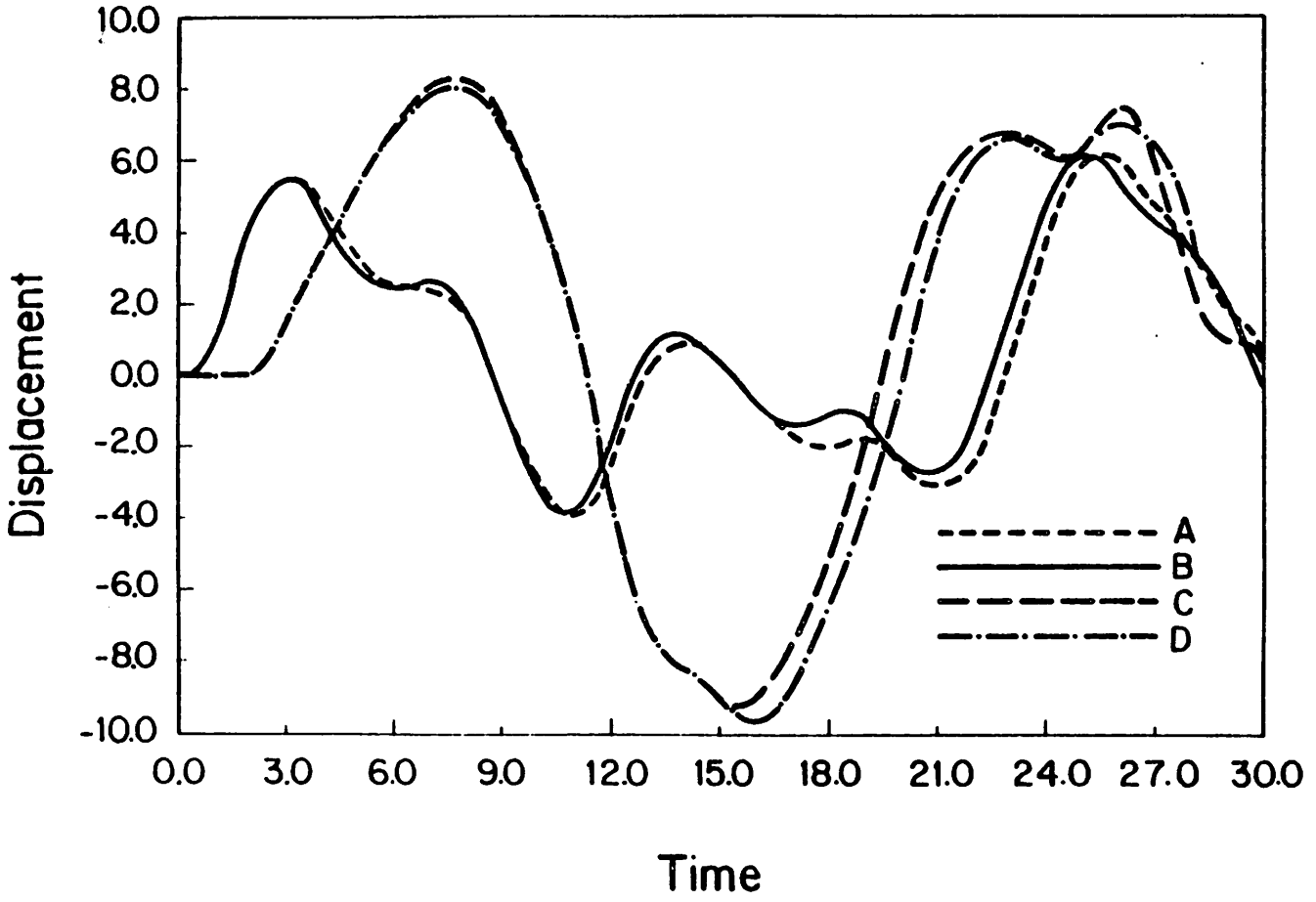

Figure 5.2.2 *Right angle cantilever beam* subject to out-of-plane loading. Time histories of elbow displacements; Line A: 2 elements, line B: 10 elements. Time histories of tip displcement; Line C: 2 elements, line D: 10 quadratic elements.

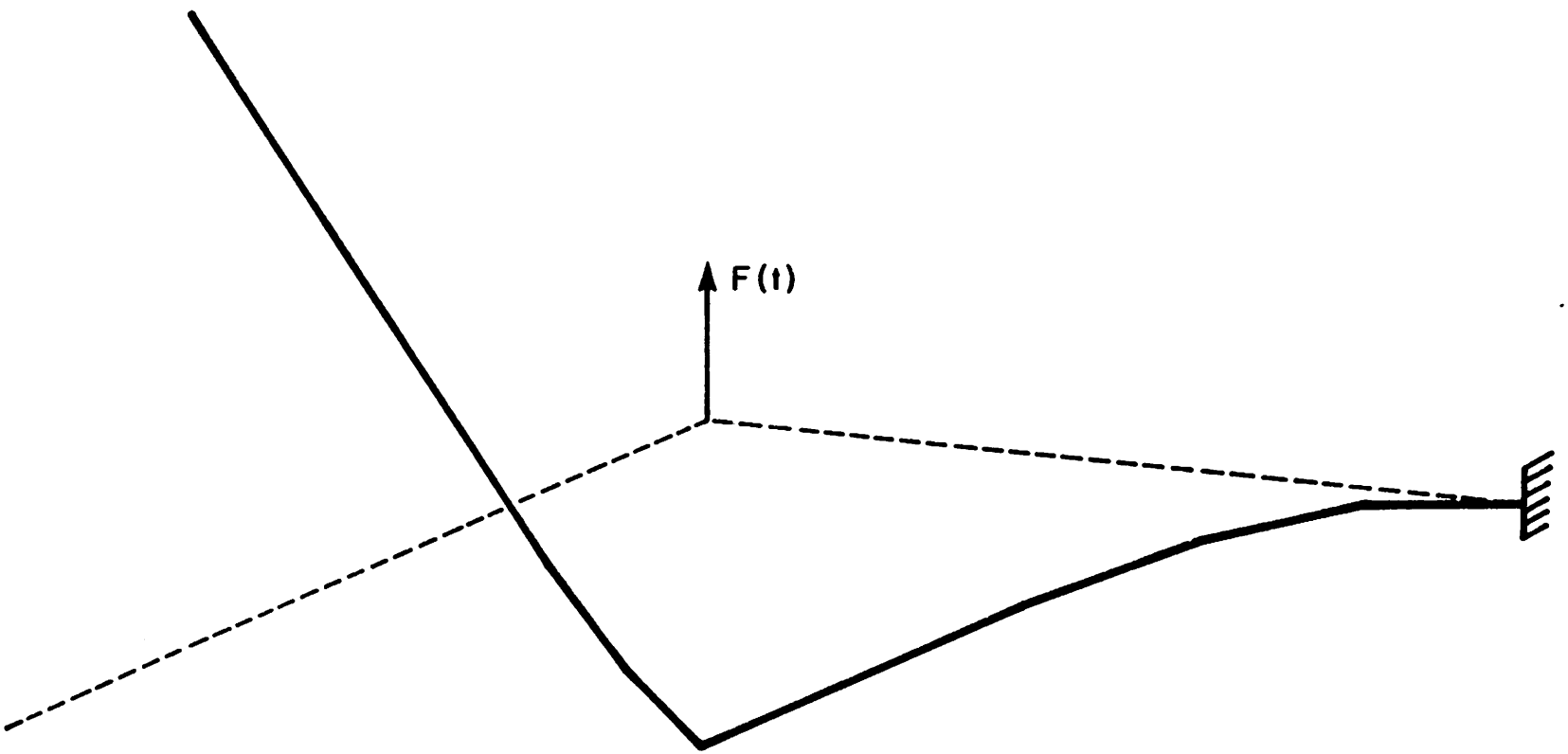

Figure 5.2.3 *Right angle cantilever beam* subject to out-of-plane loading. Perspective view of deformed shape.

Material Properties:

$GA_1 = GA_2 = 5 \times 10^6$

$EA = 10^7$

$EI_1 = EI_2 = GJ = 833333$

$A\rho = 1$

$I\rho(1,1) = I\rho(2,2) = 10$

$I\rho(3,3) = 20$

F.E. Mesh: 8 linear elements

Time History of Follower Force: $F(t) = 100\,t$

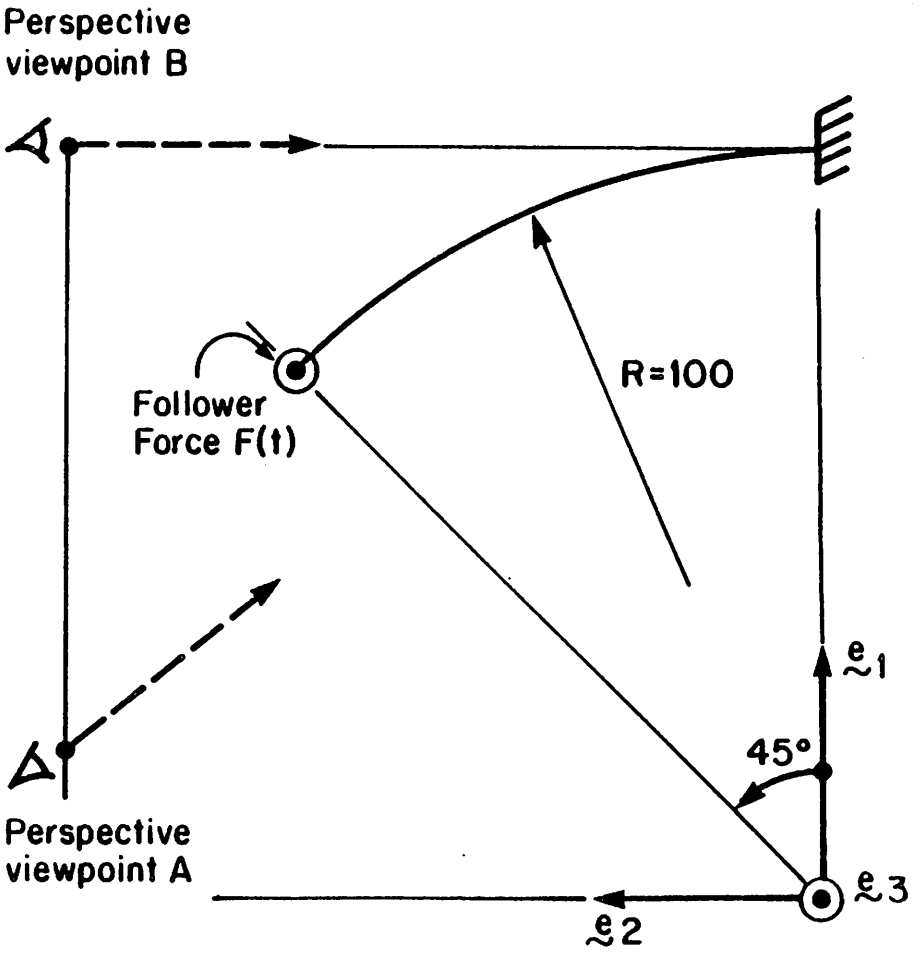

Figure 5.3.1 *Fluttering of a 45-degree bend* under follower load. Problem data.

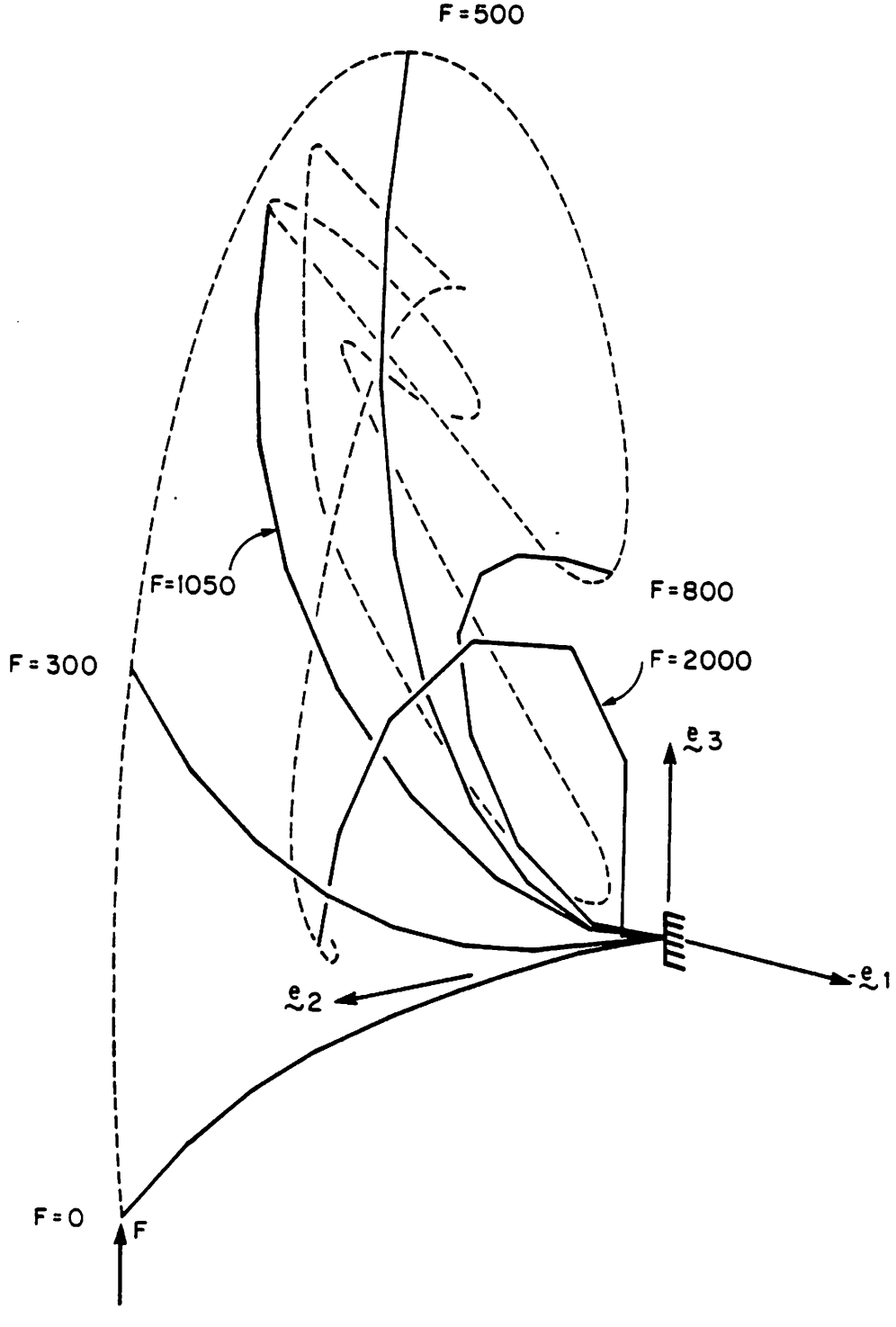

Figure 5.3.2 *Fluttering of a 45-degree bend* under follower load. Perspective view of deformed shape from viewpoint A.

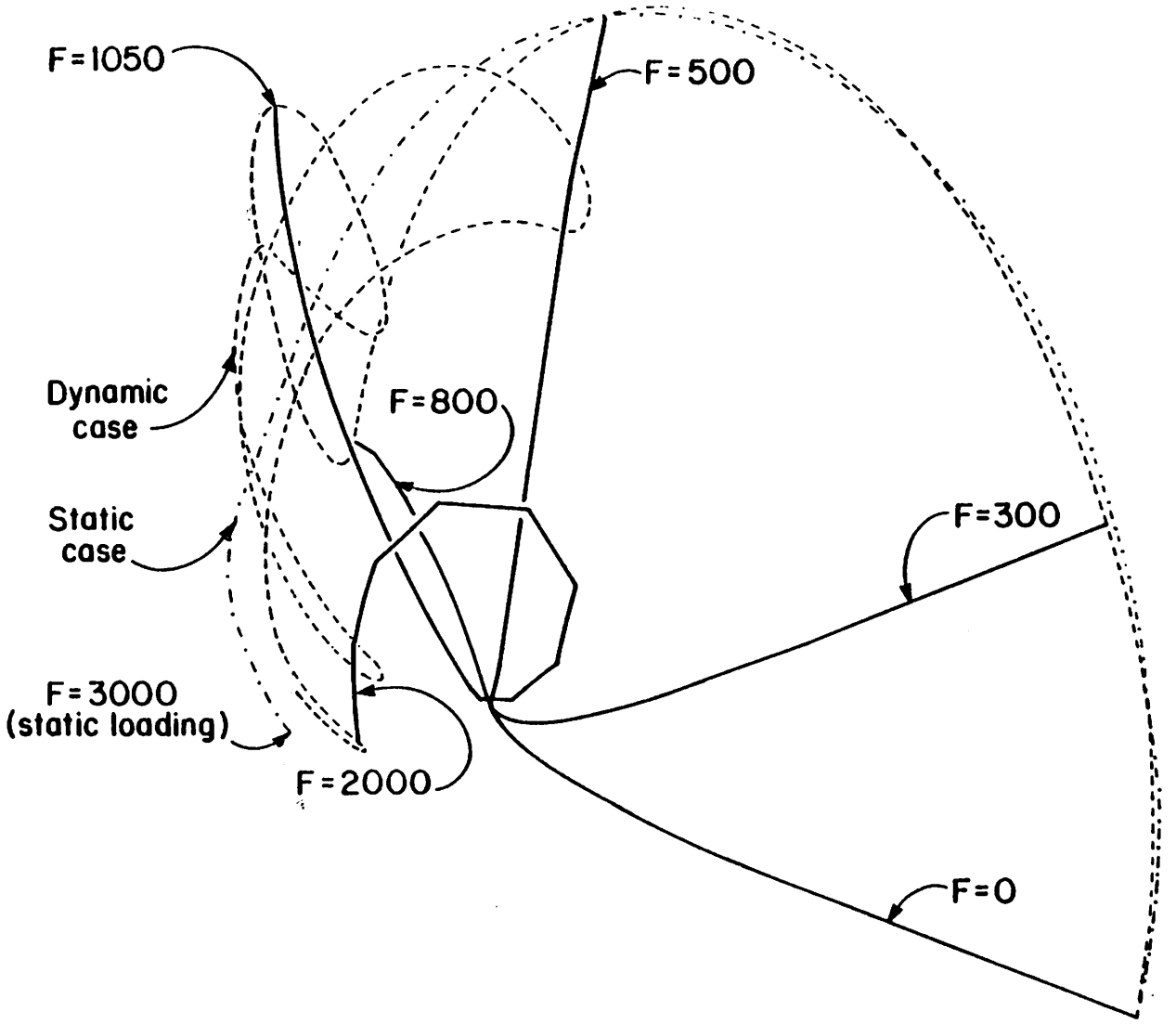

Figure 5.3.3 *Fluttering of a 45-degree bend* under follower load. Perspective view of deformed shape from viewpoint B.

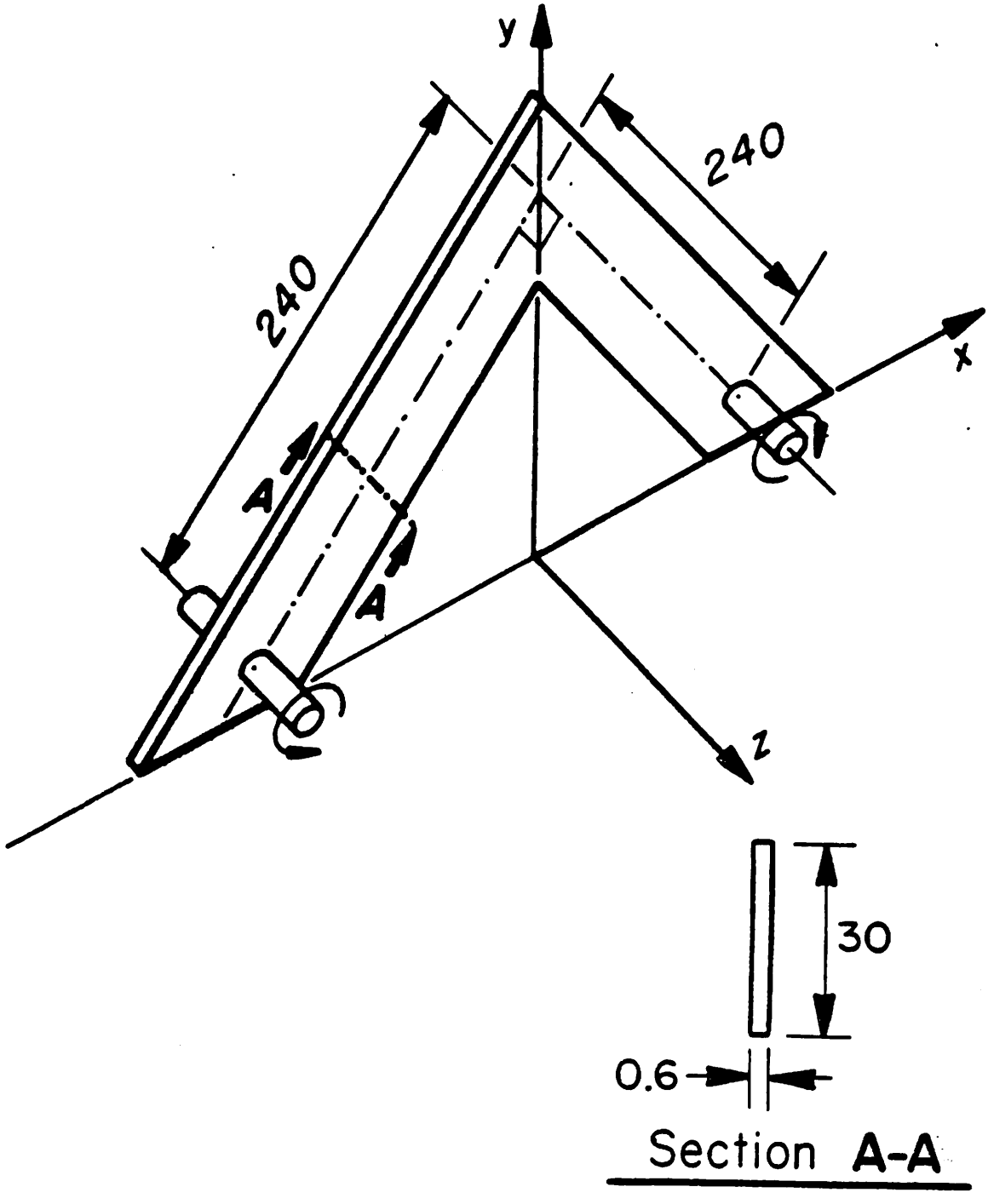

Figure 5.4.1 *Out-of-plane dynamic snap-through of a right-angle frame.* Problem data.

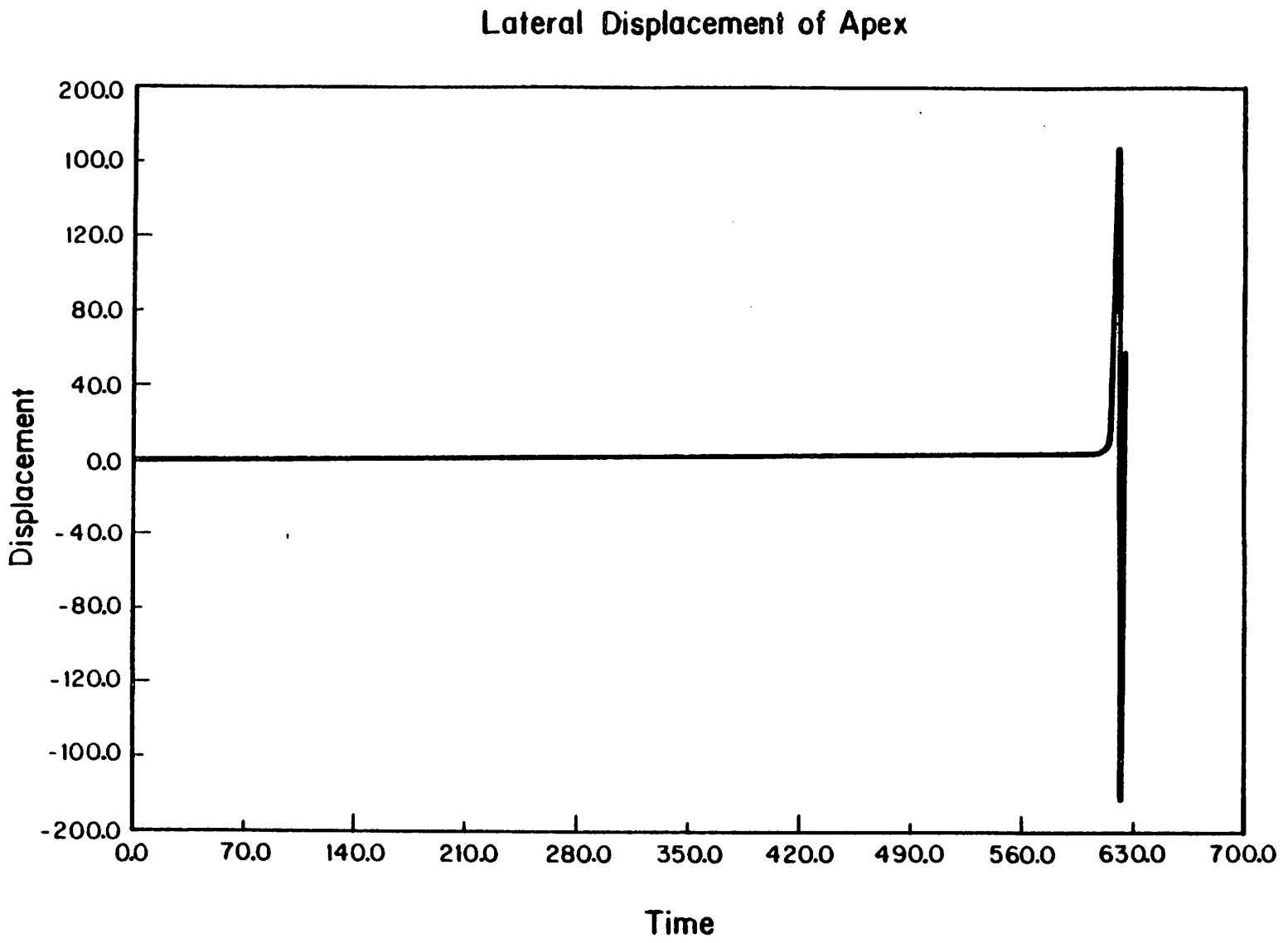

Figure 5.4.2 *Out-of-plane dynamic snap-through of a right-angle frame.* Time history of lateral apex displacement.

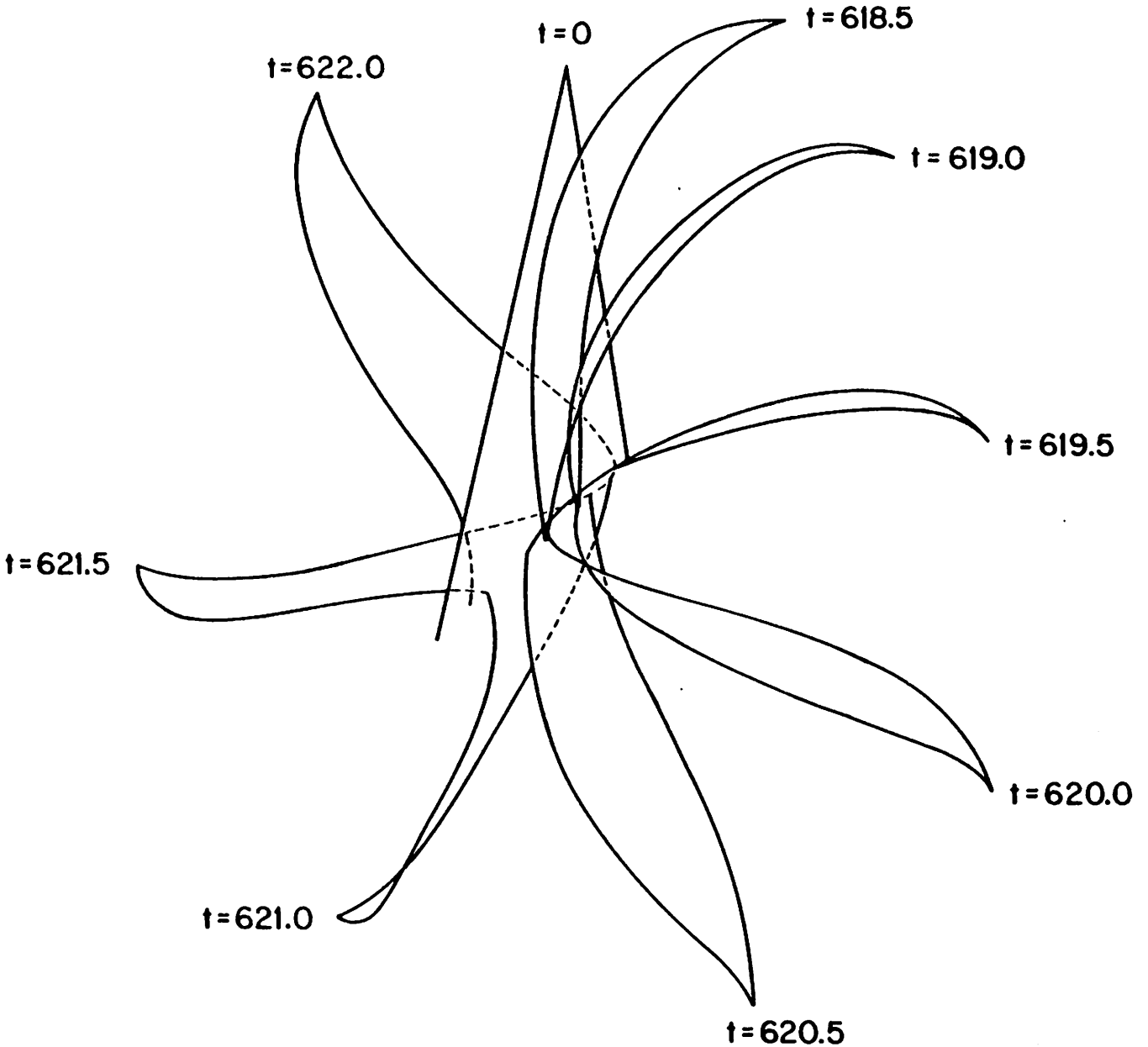

Figure 5.4.3 *Out-of-plane dynamic snap-through of a right-angle frame.* Perspective view of deformed shapes.

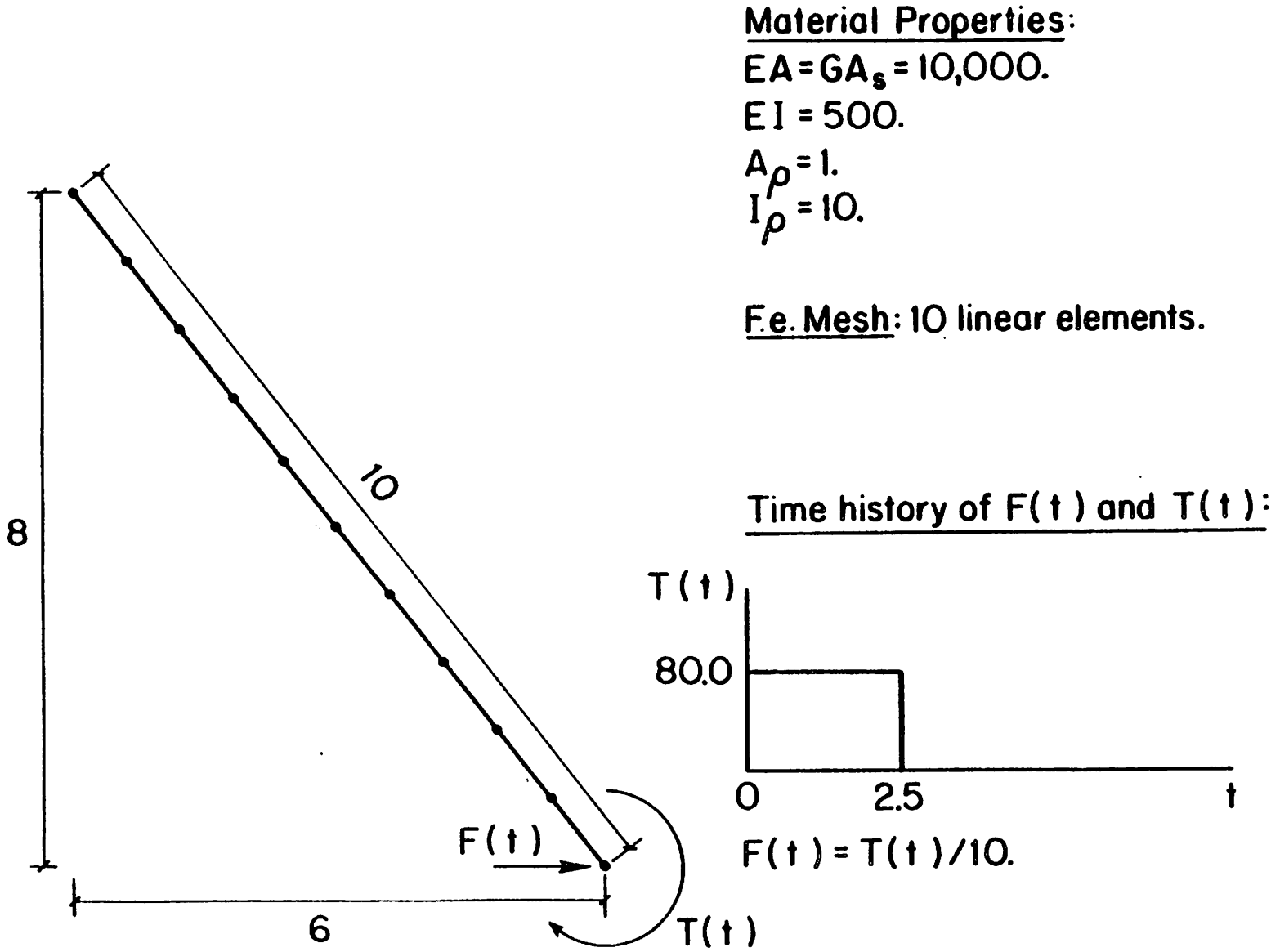

Figure 5.5.1 *Free-free flexible beam undergoing large overall motions.* Problem data.

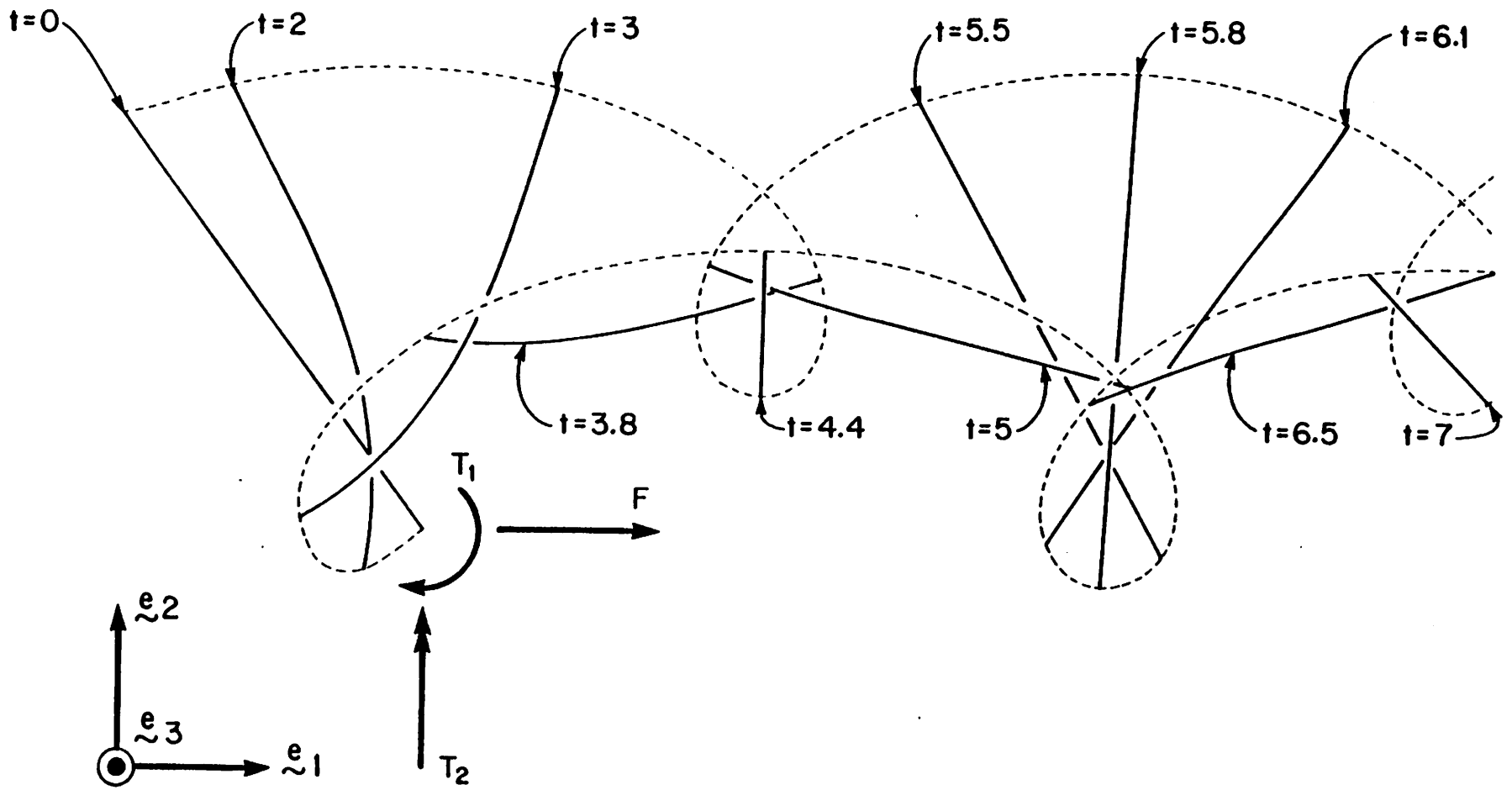

Figure 5.5.2 *Free-free flexible beam undergoing large overall motions.* Early tumbling stage.

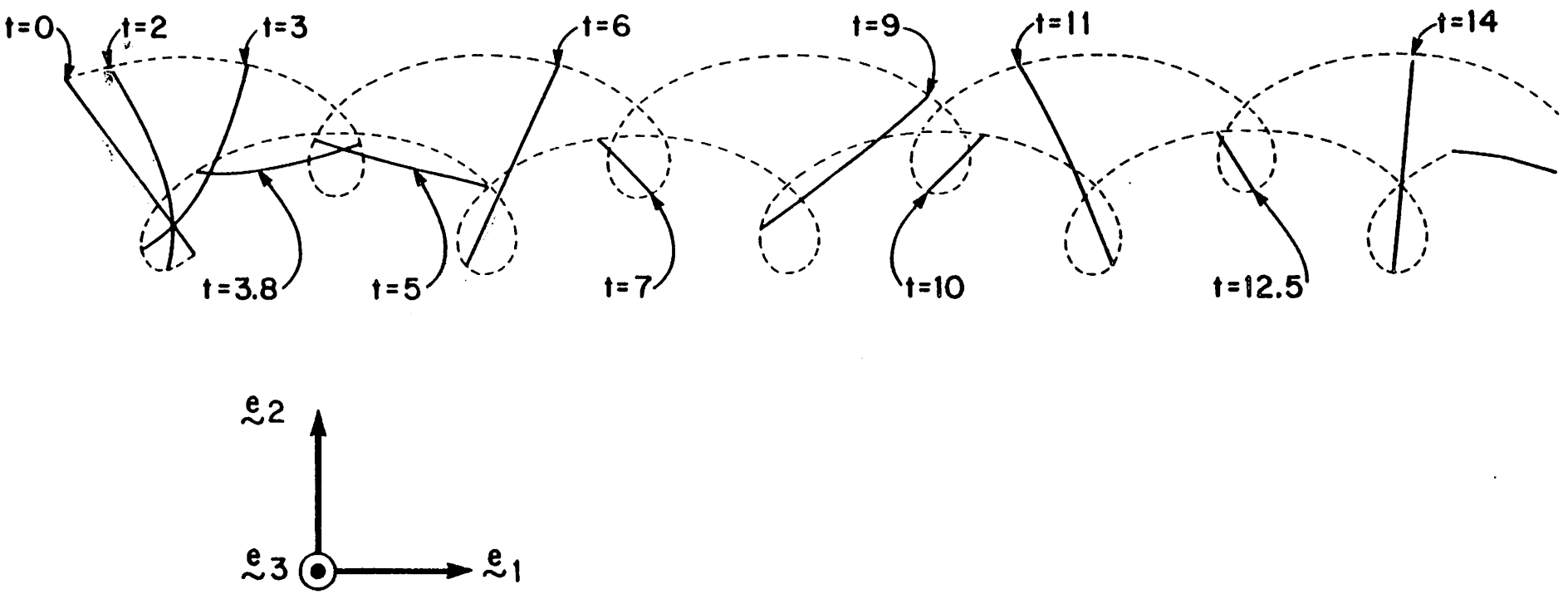

Figure 5.5.3 *Free-free flexible beam undergoing large overall motions.* Entire sequence of motion.

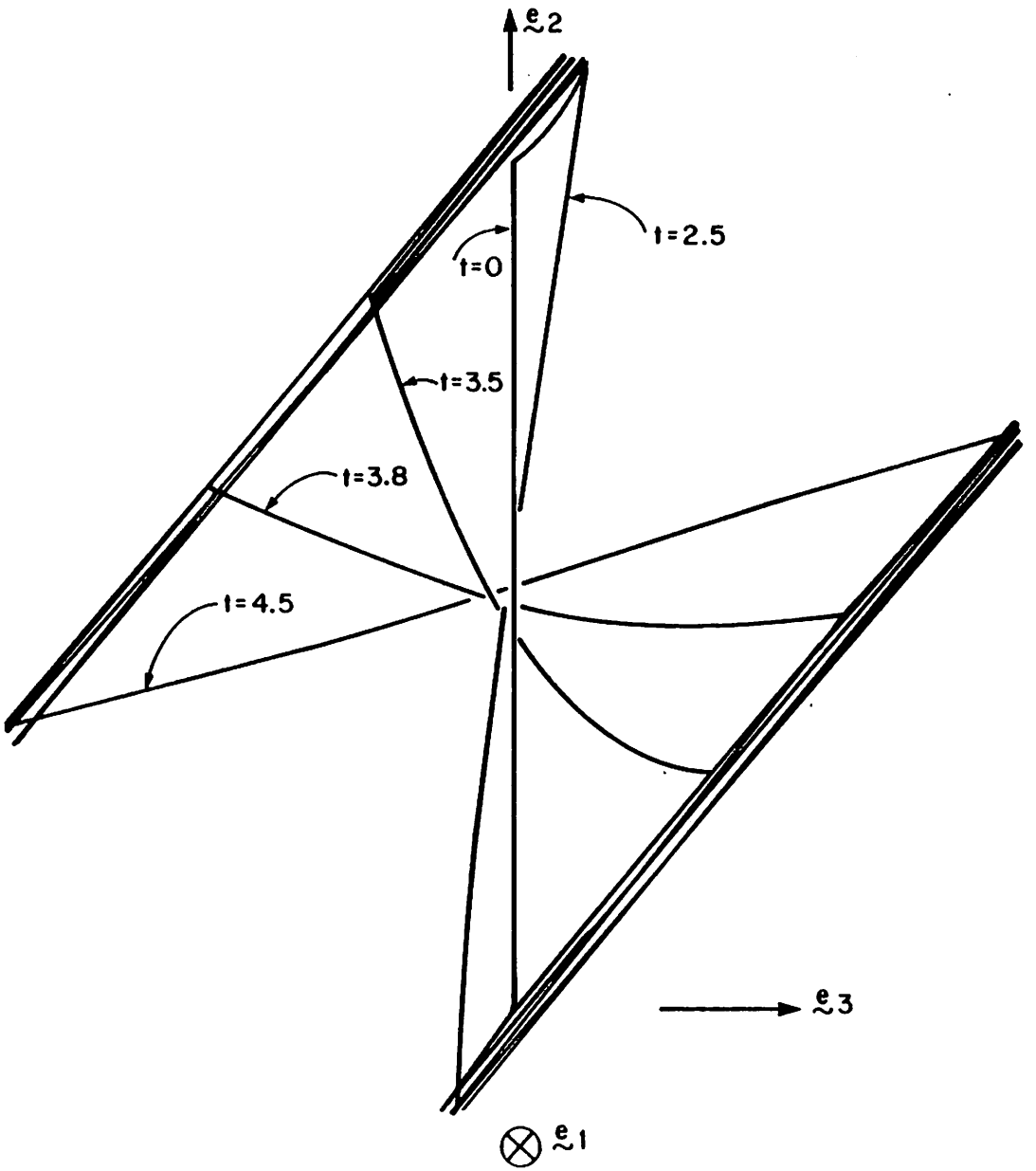

Figure 5.5.4 *Free-free flexible beam undergoing large overall motions.* Side view of deformed shapes.

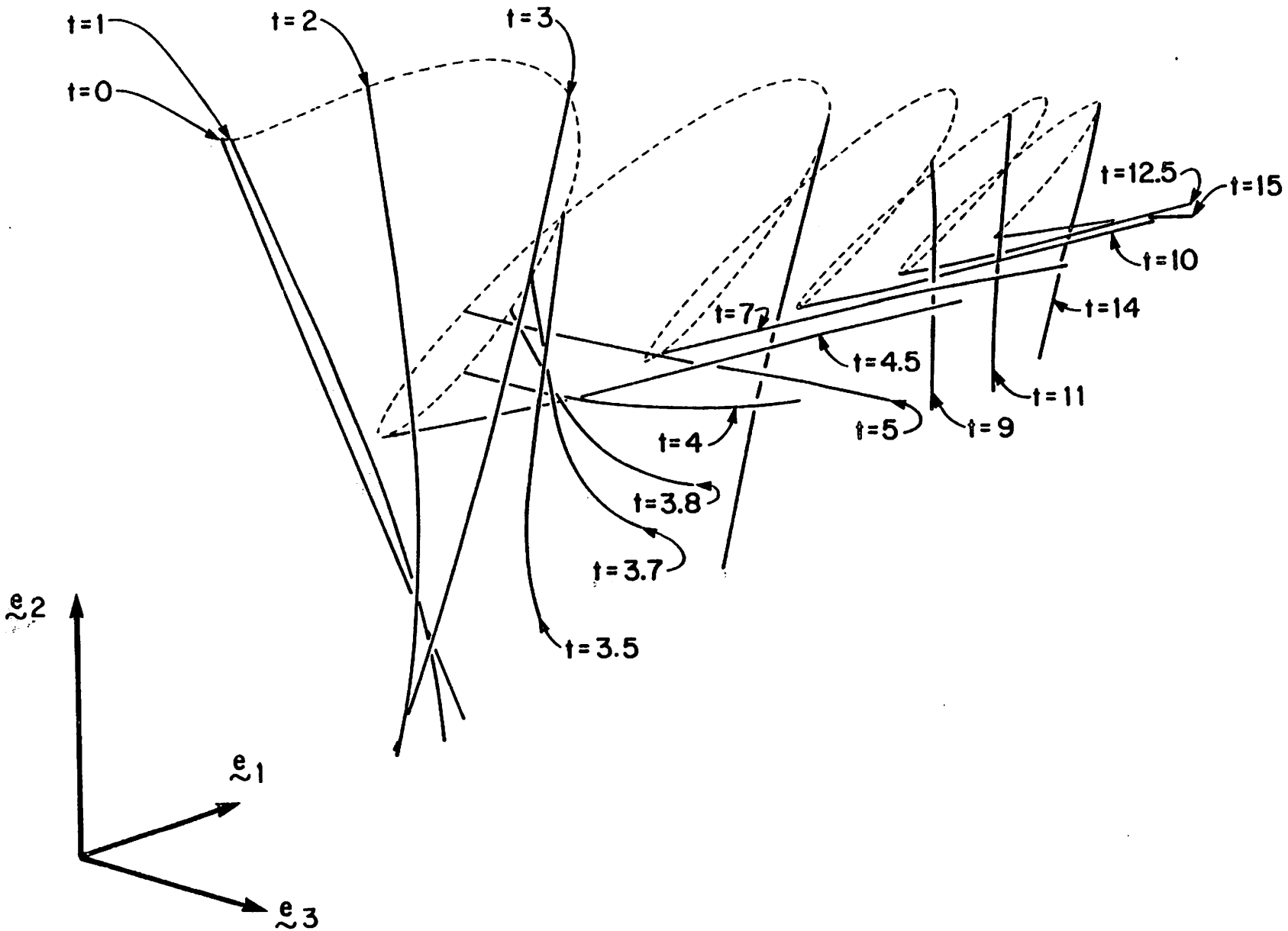

Figure 5.5.5 *Free-free flexible beam undergoing large overall motions.* Perspective view of deformed shapes.